A MODEL H.V.D.C. LINK

by

Robert Ian Dudley Riches

B.Sc.(E.E.), U.M.I.S.T. 1968

A THESIS SUBMITTED IN PARTIAL FULFILMENT OF

THE REQUIREMENTS FOR THE DEGREE OF

MASTER OF APPLIED SCIENCE

in the Department

of

Electrical Engineering

We accept this thesis as conforming to the
required standard

THE UNIVERSITY OF BRITISH COLUMBIA

April 1974

In presenting this thesis in partial fulfilment of the requirements for an advanced degree at the University of British Columbia, I agree that the Library shall make it freely available for reference and study. I further agree that permission for extensive copying of this thesis for scholarly purposes may be granted by the Head of my Department or by his representatives. It is understood that copying or publication of this thesis for financial gain shall not be allowed without my written permission.

Department of ELECTRICAL ENGINEERING

The University of British Columbia
Vancouver 8, Canada

Date April 30th 1974

ABSTRACT

This thesis presents the design and implementation of a physical model of a high voltage d.c. link to the extent that the steady state mathematical model may be validated. A conventional control system was implemented using an analog computer and featuring a new method for the detection of inverter extinction angle. A commercial 'equal angle' firing circuit was found to be a major limitation.

An attempt was made to validate a steady state linearized continuous mathematical model using a method of analysis devised by Siljak, an extension of the Mitrovic method. The often made linear continuous assumption was found to be valid only for small bandwidth systems, in which case theoretical and experimental behaviours agree.

TABLE OF CONTENTS

ACKNOWLEDGEMENT

This thesis is dedicated to the late Dr. Frank Noakes whose idea of a Trans-Canada H.V.D.C. Link may yet become a dream realized.

I should like to thank my other two supervisors, Dr. B. Kabriel and Dr. H. Cheann for their encouragement and advice. Special thanks are due to Tilly Martens for her typing, Joe Hosie and Don Lumley for their proof reading, and many friends, especially Dr. H. Moussa who provided many interesting insights.

I also acknowledge a Research Assistantship 1968-70 and the forebearance of the Department of Electrical Engineering.

1. INTRODUCTION

The economic feasibility and technical applicability of h.v.d.c. transmission in certain fields of application have now been established in a number of h.v.d.c. schemes throughout the world. In long distance bulk power transmission[1,2,3], underground[4] and submarine cables[5,6] and transfer of power between systems of different frequency[12], h.v.d.c. transmission has been used to great advantage.

As operating experience increases, more refined control systems[13,14] provide the possibility for h.v.d.c. transmission to move into new fields of application: such as the use of h.v.d.c. as a stabilizing element in parallel a.c. - d.c. systems[7,15], and multi-terminal[16] d.c. systems which would allow more effective use of economic generating capacity, for example, to supply areas within different time zones.

Modelling provides a scope for experimentation and development that the full-sized commercial installation cannot provide due to the high cost of capital equipment and the sometimes unknown, possibly destructive tendencies of certain tests. Existing physical models of h.v.d.c. transmission systems range in size from micro-[17,18] through medium-power[19] to the full size experimental d.c. link developed by a leading manufacturer in h.v.d.c. equipment.

The distinction between physical and mathematical models is an important one[20]: a small-scale physical dynamic model, replicating, as far as possible, per-unit quantities, time constants and behaviour of the full-sized model provides valuable practical experience that a mathematical model may be used to describe. On the other hand, a satisfactory mathematical description allows measures of performance, certain predictions of behaviour and further model refinements to be made according to prescribed techniques.

A similar approach is adopted in this thesis in developing a small scale physical model of a h.v.d.c. link with conventional control systems. The model scale was chosen to be compatible with existing micro-machine laboratory models. The model link was built, tested, and a mathematical model developed according to certain assumptions. In this study one such assumption is critically examined: that the converter system may be represented mathematically as a linear continuous system.

One of the more important[24] measures of system performance is stability, and the particular emphasis of this study is relative stability. The mathematical statements of stability criteria in linear continuous systems are well known; the analysis may be divided into two categories: closed form solutions in the algebraic domain and the open form time domain solution of the differential equations.

For this study the former was chosen since the closed form solution facilitates relating the physical system parameters to the theoretical solutions. Other studies include Eriksson[22] et alia, applying Nyquist's criterion to a mathematical model, and Clade and Lacoste[23] were able to compare the application of Routh's criterion to the results obtained from a small experimental model.

The mathematical model in this thesis is developed from a practical model d.c. link. The design considerations for the physical model are outlined in Chapter 2, the construction and testing in Chapter 3. A steady-state theoretical model is derived and analysed using a parameter plane technique devised by Siljak[24,25,26]. The method of

Siljak is a graphical mapping procedure which allows specific s-plane contours to be mapped onto the parameter plane of two adjustable system parameters appearing in the coefficients of the characteristic equation. This effectively allows the locations of the roots of the characteristic equation to be confined within these contours by appropriate adjustment of the parameters. In addition, a method for computing the coefficients of the characteristic equation is developed by the author.

Following the development of the experimental model, the constant extinction angle and constant current controllers for the inverter are analyzed using Siljak's method. The parameter plane maps are used to effect parameter adjustment for best relative stability and to illustrate the validity of the linear continuous assumption. A new method for the detection of inverter extinction angle is presented in Chapter 4.

2. DESIGN CONSIDERATIONS FOR A D.C. LINK

This chapter describes the components of a h.v.d.c. link, shown in Fig. 2.1, and their behaviour which the model must accurately reflect. While the control system of a commercial d.c. link encompasses many refinements, the basic control systems for steady state operation are described here since they represent the minimum requirements for the normal regulation of a link.

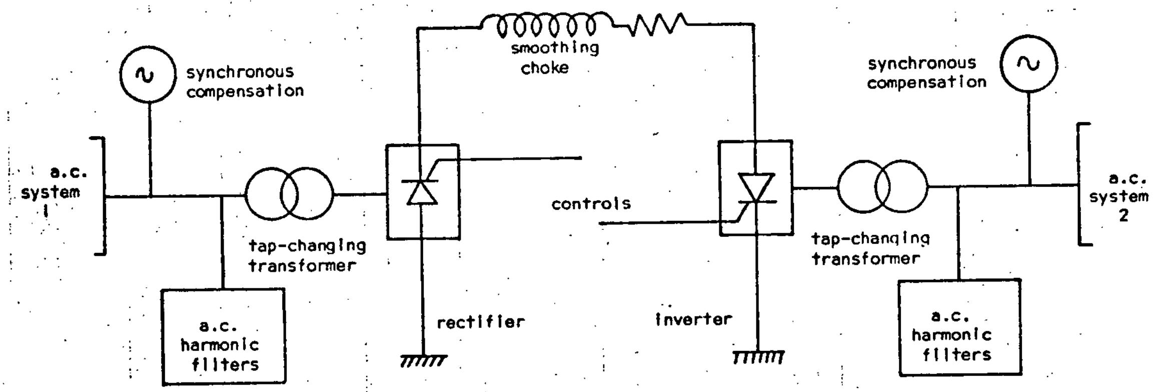

Fig. 2.1. Schematic d.c. Link, showing each component

2.1 The Converter

The converter is a static switching device which, by switching appropriate segments of a three-phase a. c. supply, permits the conversion of power from alternating to unidirectional, and vice versa. The quality of the direct voltage profile, characterised by the imposed ripple, depends upon the number, connection, and firing delay of the phase-controlled rectifying elements used, and the number of phases of the supply. The most common connection used in h.v.d.c. transmission is the six-pulse bridge circuit, Fig. 2.2a, which is known to maximize valve and transformer utilization. Other possible connections are covered extensively in Hancock[28] and Schaeffer[29].

Valve utilization is based upon the proportion of the cycle that the valve spends in conduction, which affects the rating, and the fraction of the total output current carried by each valve when in full conduction. Transformer utilization is based upon the required ratings of primary and secondary windings, as determined from the current waveform in each winding.

Pairs of bridge units are connected in series and phase shifted with respect to each other by 30° to form a unit with output ripple of 12 pulses per cycle. These 12-pulse units are themselves connected in series to produce the high voltage required to make d.c. transmission economical[30]. However, a satisfactory representation of converter behaviour is obtained with the use of a single 6-pulse bridge unit[31].

While mercury arc valves are used in commercial installations, it is impractical to use them on a small scale model. The bridge elements used in this model are silicon controlled rectifiers, solid state devices which have the same operating characteristics as mercury arc rectifiers - conductive in forward direction only and conduction may be blocked until a pulse is delivered to the gate.

Rectifier waveforms are shown in Fig. 2.2: the direct output voltage, V_{dr}, is the average value of the voltage envelope shown in bold outline in Fig. 2.2(b); the numbers refer to the conducting valve of the bridge circuit shown in Fig. 2.2(a). Voltage control is effected by variation in firing angle α; so that an increase in α increases the volt-time area 'A', Fig. 2.2(b), resulting in a decrease in average voltage. A further volt drop, shown by volt-time area 'B', is caused by the commutation process:

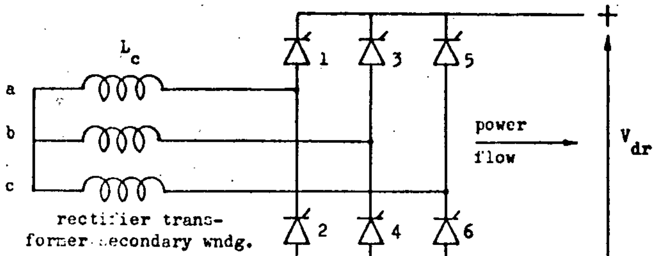

(a) rectifier bridge circuit

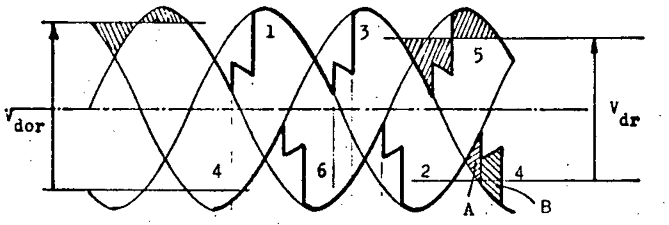

(b) rectifier direct output waveform with respect to secondary neutral

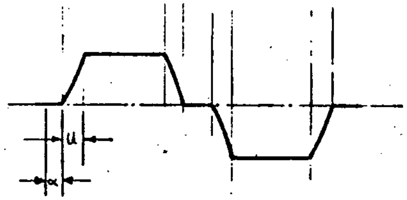

(c) a.c current waveform in phase 'a'

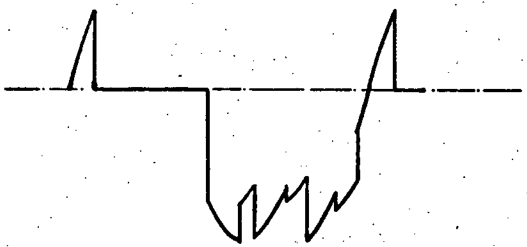

(d) commutating voltage of valve 1

Fig 2.2 Rectifier Waveforms

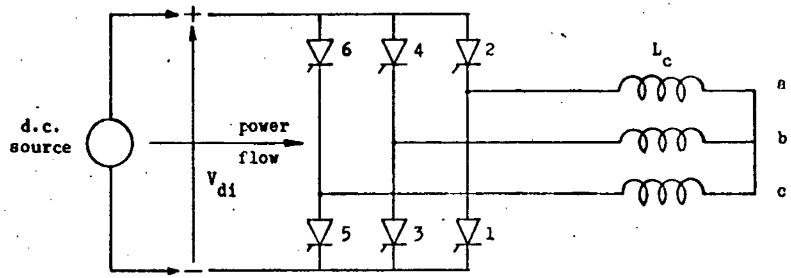

(a) Inverter bridge circuit and secondary transformer winding

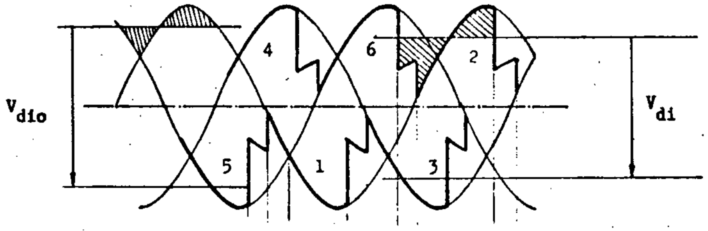

(b) Inverter d.c waveform with respect to secondary neutral

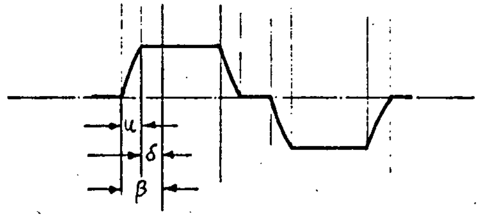

(c) current waveform in phase 'a'

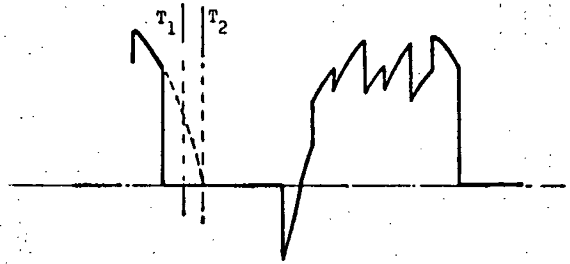

(d) Commutating voltage of valve 1

Fig 2.3 Inverter Waveforms

in h.v.d.c. converter operation, commutation occurs naturally, i.e. current transfers to the anode of the next valve because, at the instant of firing, the potential at the anode of the new valve is higher than that at the anode of the conducting valve. Due to the leakage reactance L_c per phase of the converter transformer, the extinction of current in the conducting valve cannot occur instantaneously, but over a short period of angular duration u°. During this period, two valves on the same side of the bridge are conducting, giving the appearance of a short circuit between phases. The entire voltage for each phase is absorbed in the leakage reactance, and the output voltage during commutation is the mean voltage between these two phases. The commutation voltage of a valve is the voltage between anode and cathode, shown in Fig. 2.2(d) for valve 1.

Inverter waveforms are shown in Fig. 2.3: the firing angle, advanced to $\alpha > 90°$, minimum α for inverter operation, is more conveniently known as the 'angle of advance' $\beta = \pi - \alpha$. From Fig. 2.3(d), the commutating voltage for valve 1, it may be seen that the instant of firing occurs towards the end of the period of positive commutating voltage. For successful commutation, the preceding valve 5 must be extinguished, T_1, before the end of this period, T_2, after which time commutation cannot be completed or initiated. After extinction, the valve must de-ionize before it becomes non-conducting. The margin or extinction angle δ, provides a safety margin between extinction and end of positive commutating voltage to allow for de-ionization and control system inaccuracies and assure successful commutation.

2.2 Grid Control Firing Circuit

In the basic bridge unit, the six valves are fired in the correct sequence by gate pulses at nominal intervals of 60° electrical, controlled in phase to produce the firing angle α. The overall control system is usually divided physically into two parts.

(a) the pulse unit which forms and times the delay according to the input signal from the

(b) controller i.e. reference, feedback and error amplifiers.

While the later chapters deal with the controllers and the mathematical analysis of behaviour, there are two basic approaches to delay timing in the design of pulse units:

(i) 'Equal Angle', the conventional scheme; where, in the case of the 3-phase bridge, six independent delay circuits time the delay of each firing pulse from a fixed reference point on the corresponding phase voltage.

(ii) 'Equal Space', a contemporary scheme invented by Ainsworth[13], where each firing pulse is timed at 60° electrical after the preceding pulse for steady state. A change in α is made by momentarily perturbing the frequency of the 360 hz pulse train.

In either case it is desirable that the firing pulse itself has a duration equal to the conduction period of the valve. This forestalls the synchronization problem which may otherwise be encountered during start-up[17].

2.3 Reactive Power Compensation

The transformer secondary current waveform, as shown in Fig. 2.2 is decidedly non-sinusoidal in nature; there are two effects.

(i) The injection of a.c. harmonic currents and voltages into the a.c. system can have deleterious effects upon communication circuits[32], cause overheating in highly inductive circuits[36] and, under certain conditions[34] cause harmonic instability.

(ii) Even with no phase delay the power factor is necessarily less than unity; with the introduction of firing delay the power factor is further reduced: reactive power is consumed, i.e. lagging reactive volt-amps are absorbed.

From inspection of the relative phase displacement of the transformer secondary current with respect to voltage, Figs. 2.2(b),(c) it is evident that the rectifier absorbs lagging VARs. That the inverter absorbs reactive power from the receiving a.c. system may be shown thus: the voltage and current waveforms for one phase at the a.c. terminals of the inverter are shown in Fig. 2.4(b). By considering the inverter as an a.c. system load element, defined in Fig. 2.4(a), the power in the load may be written from the phasor diagram Fig. 2.4(c)

$$S = VI^* \text{ or } S^* = V^*I$$

$$S^* = |V|\varepsilon^{-j\theta} \cdot |I|\varepsilon^{j(\pi + \theta + \emptyset)}$$

$$= |V| \cdot |I|\varepsilon^{j(\emptyset + \pi)}$$

$$= |V| \cdot |I|\{-\cos \emptyset - j \sin \emptyset\}$$

$$S = |V| \cdot |I|\{-\cos \emptyset + j \sin \emptyset\}$$

$$= -P + jQ$$ i.e. supplying real power and

receiving VARs where $V = |V|\varepsilon^{j\theta}$, $I = |I|\varepsilon^{j(\theta + \pi + \emptyset)}$, and $\emptyset$ as shown in Fig. 2.4(c)

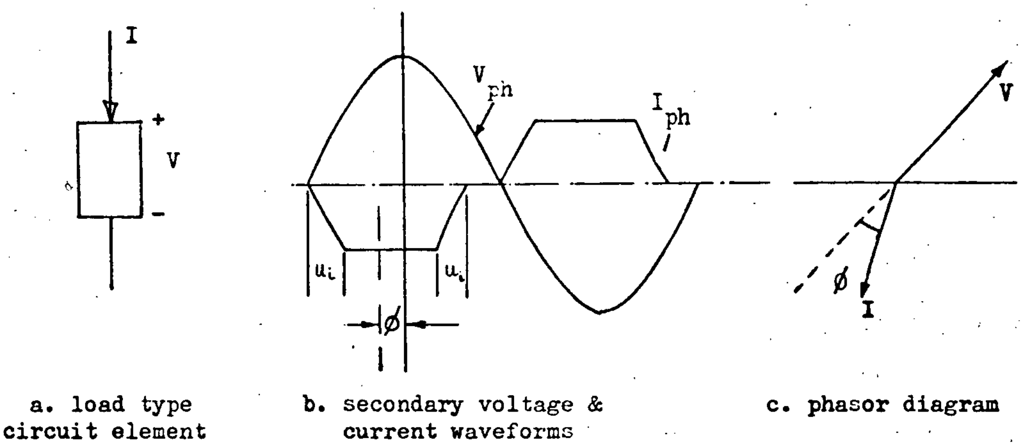

Fig 2.4 Power at the Inverter

Fig. 2.5 illustrates the reactive power requirement of a rectifier and its variation with firing angle α and commutating reactance X_{cr} for a direct power output of 1 p.u.. Typical[8] values for commutating reactance and firing angle are 0.15 p.u. and 20°; for which 1 p.u. output power requires 0.67 p.u. reactive power

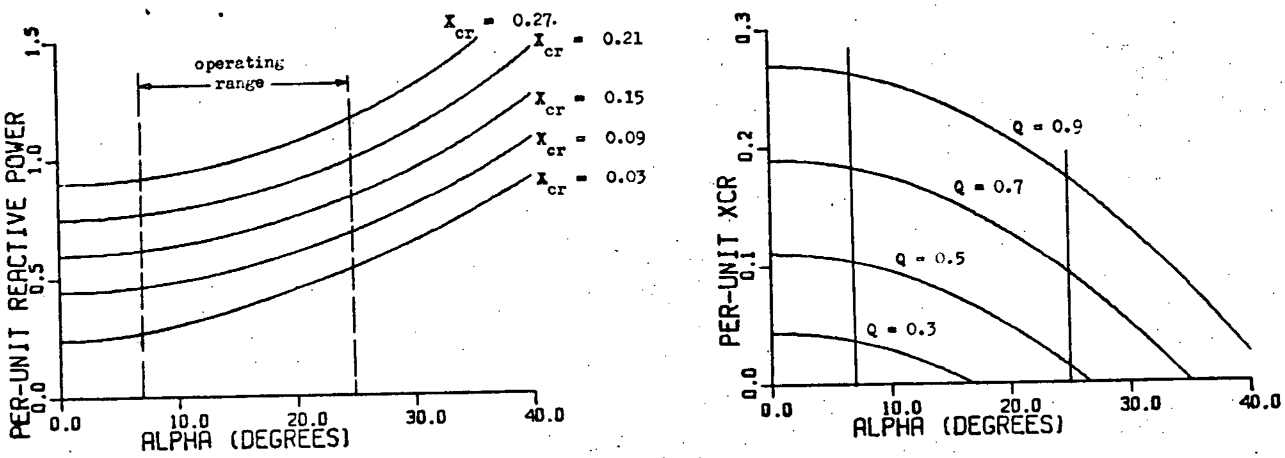

Fig 2.5 Reactive Power Demand of Rectifier

Fourier analysis resolves the transformer primary current into harmonics of number $6n \pm 1$, $[n = 1,2,\ldots.]$, and the peak fundamental current to be $\frac{2\sqrt{3}}{\pi} I_d$ [33]. Changes in firing angle and commutation angle result in slight changes in amplitude and frequency content of the harmonics, and firing pulse timing errors bring in small amounts of non-theoretic harmonics. However, Read[35] has shown that the amplitude of the fundamental is essentially unchanged. In analytical studies, the a.c. current is assumed to be sinusoidal with constant amplitude over changes in α.

Tuned filters provide a low impedance path to ground for these harmonic currents, and attenuate the harmonic voltages to provide an acceptable level of distortion of the fundamental[33]. At fundamental frequency the tuned filters appear capacitive, and provide some of the reactive power required by the converter. By carefully selecting the inductive and capacitive component values, the full load reactive power requirement may be met solely by the filter[38]. Fig. 2.5 shows the variation in demand for reactive power with respect to firing angle and commutating reactance. However, in this case the amount of reactive power supplied by the filter remains fixed, and the excess VAR at low converter load is fed into the a.c. system. If this causes excessive regulation at the inverter terminals, then the filter size must be reduced and additional reactive power compensation provided, either by series capacitors[39] or synchronous condensers[40].

Voltage regulation at the converter depends upon the dynamic characteristics of the a.c. system[38]. Hence it may be seen that the design of filters and compensation equipment, and the optimal balance of reactive power supplied by each depends upon the characteristics of the a.c. system to which it is appended.

2.4 D.C. Transmission System

Depending upon the number of converters, there exists a choice of transmission configurations: one-pole, ground return or two-pole. The one-pole configuration is adequate for modelling most situations, and was used in the present model.

Also, the inductance of a d.c. line, based upon the dimensions given for the Nelson River Line[50] indicate small values of inductance for a model PI-section representing 100 mile sections. The values were very small compared to the value of smoothing reactor inductance and were consequently ignored since the scope of this study did not embrace the investigation of d.c. line faults.

2.5 Operation and Control of a D.C. Link

This section describes the principles of operation and requirements of a suitable control system for a d.c. link. The schematic diagram of the link is shown with the basic components of its control system in Fig. 2.6.

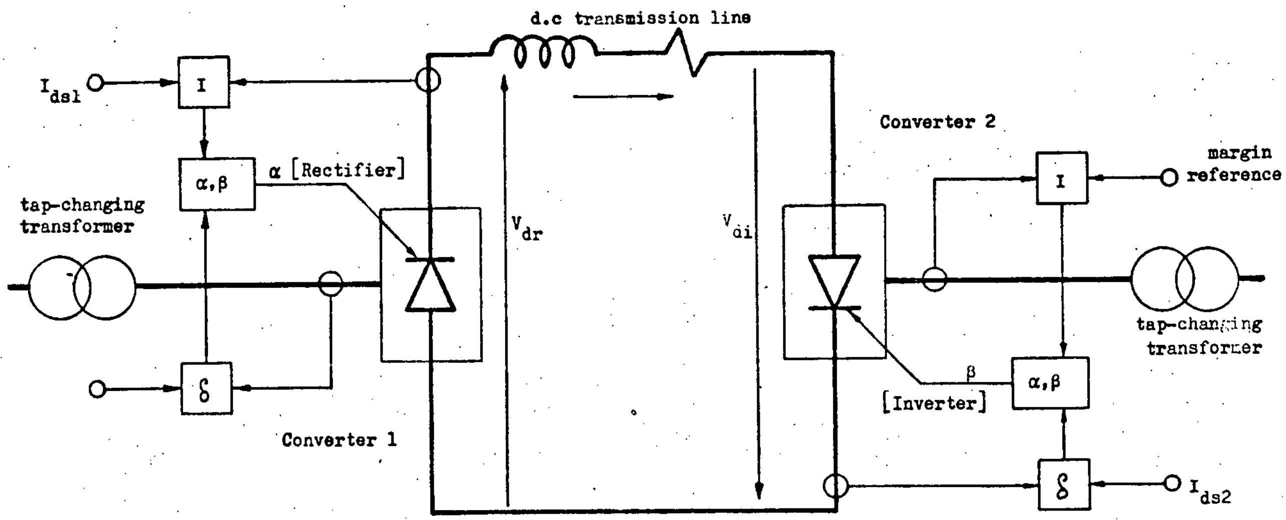

Fig 2.6 Schematic Unipolar d.c link

While d.c. links operate with considerable margin with respect to the power limit, the possibility does not exist[41], as is normally the case with a.c., of transferring power far above the design economic level. This arises from the fact that present converter equipment cannot be overloaded - there are definite limits to the voltage and current handling capabilities of converters which, if exceeded, result in the destruction of the valves. Hence a certain amount of converter protection is built into the control system.

The usual mode of control for the rectifier[37] is a constant current regulator, so that if the current exceeds the set value, control action increases the firing angle, decreasing the direct output voltage, and thus preventing the output current rising above the set value. On the other hand, the inverter control must ensure that the commutation and mercury vapour de-ionization is complete before the commutation voltage becomes negative, Fig. 2.3(e). Usually the firing angle is changed in such a manner as to keep the extinction angle δ_o constant. This control is known as constant extinction angle (c.e.a.) control.

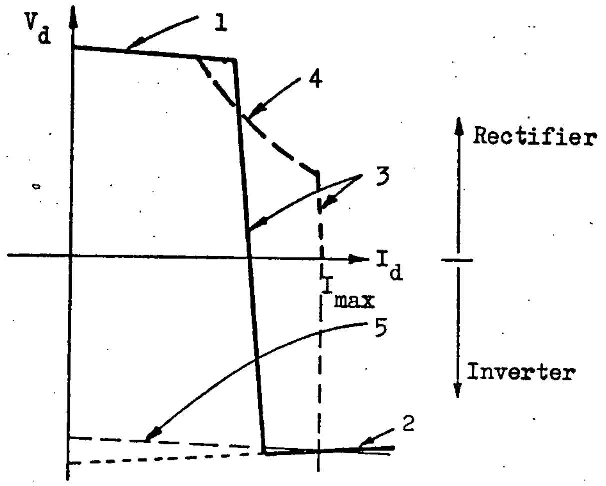

Fig 2.7 Control Characteristic of Converter

The control characteristic with these minimum requirements in Fig. 2.7 consists of three sections:

(1) The natural voltage characteristic of the rectifier is the regulation characteristic of the converter with firing angle α held at its minimum value. The slope depends upon the value of commutating reactance.

(2) Constant extinction angle (c.e.a.) control allows the inverter to operate at minimum angle of advance, allowing for a safety margin. While it does not protect the inverter from over-currents, it does prevent commutation failure.

(3) Constant current (c.c.) control is provided for both rectifier and inverter; for the rectifier, the control action in response to a rise in line current above a preset reference I_{ds1} is to further delay α, reducing the rectifier output voltage and therefore current; for the inverter, should the line current fall below I_{ds2} then the angle of advance β is made larger than that required to maintain constant extinction angle.

Constant power (c.p.) control is an alternative mode of control for both rectifier and inverter characteristic (4) in Fig. 2.7 in which c.c. or c.e.a. control is provided for override. Constant β control [part 5 of the characteristic] is the alternative for c.e.a. control, being the natural regulation curve of the inverter. However, an inverter is rarely operated on this characteristic.

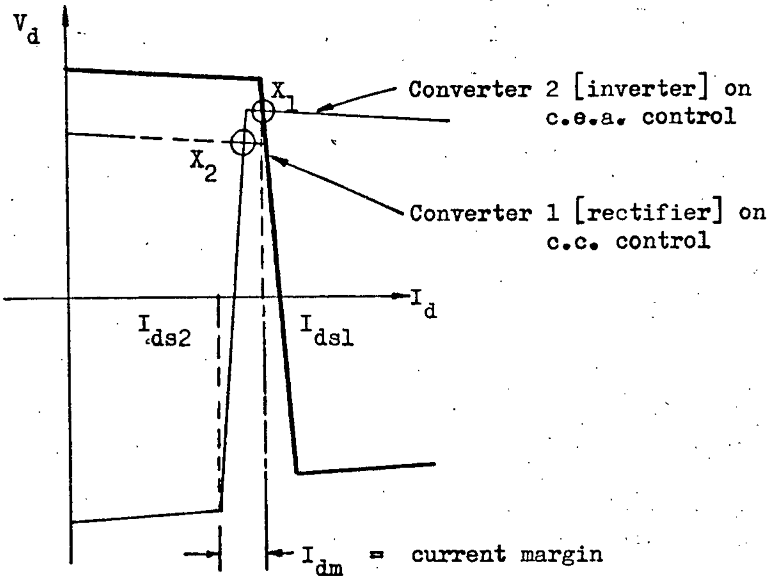

Fig 2.8 Two-converter control characteristic

For the two converter system, the current setting I_{ds1} of converter 1, see Fig. 2.6, operating as a rectifier, is greater than the current setting I_{ds2} of converter 2, operating as an inverter, by a small current margin I_{dm}, typically 20%. This margin setting has to be large enough to allow sufficient operating margin between the two constant current characteristics, in order to avoid simultaneous operation of both. Such operation is clearly undesirable and may also be very unstable. In Fig. 2.8, X_1 is the operating point with converter 1 [rectifier] operating in c.c. mode and the inverter operating in c.e.a. control mode. Converter 1 will operate as a rectifier and converter 2 as an inverter as long as current setting I_{ds1} is greater than I_{ds2}. If the a.c. system at the rectifier changes so that the natural voltage characteristic falls below the c.e.a. control characteristic of the inverter, converter 1 will still operate as a rectifier, but the constant current controller of the inverter will be activated, and the operating point changes from X_1 to X_2. The power flow in the link will not change direction unless the sense of the current margin I_{dm} is reversed.

Each converter is equipped with a tap changing transformer to ensure that the system operates in the preferred mode, i.e., the rectifier in c.c. control mode and the inverter in c.e.a. control mode. In practice the rectifier tap changer is operated to keep the firing angle, and hence reactive power demand, within specified limits. The inverter tap changer is operated to keep the d.c. line voltage at a specified level.

The change in operating point from X_1 to X_2 has resulted in the rectifier firing angle reaching its limiting [minimum] value of α. The operation of the rectifier tap changer, to increase the transformer secondary/primary turns-ratio, raises the natural voltage characteristic to above the c.e.a. characteristic of the inverter, allowing the operating point to revert to X_1.

It can be seen that a change in power transfer, and therefore current, through the link requires careful co-ordination of both converter control systems in order to maintain the current margin. In practice, a telecommunication link is maintained between the two stations, as is also some predetermined procedure to prevent shutdown of the power link in the event of a communication failure.

This chapter has described the components of a d.c. link and its basic mode of behaviour. The next chapter describes the implementation of these components. Filters have not been installed with each converter since there exists no laboratory model power system with which to operate one end of the d.c. link. Each converter therefore, is connected to the 'infinite' system.

3. CONSTRUCTION AND TESTING OF THE MODEL

This chapter describes in detail the construction of the model and the initial testing of the components. Also included are the power equations for the converter and the start-up procedure for the link.

3.1 The Converter Bridge

Two converter bridges, each consisting of one six-pulse unit, were bulit. The power rating of up to 4.5kw, maximum of 300v at 15A, allows compatibility with existing micro-machine equipment.

For the converter bridge elements, scrs' were used as their operating characteristics are similar to mercury arc rectifiers or thyratrons. They also have the advantage that the forward volt drop while in the conducting state is small and their switching time is short. In addition their size is small but the power dissipation at the junction requires that the scr be mounted on a heat sink. The circuit considerations and design rating for a specified bridge rating are as follows:

1. The current rating [average repetitive] is determined by the maximum allowable scr operating temperature. In the three-phase bridge circuit each element conducts for just over one third of a cycle: hence for a maximum rating of 15A the average repetitive current is 5A, from which may be determined the heat sink requirements.

2. Peak reverse voltage. For the bridge circuit which may be required to deliver $\sim$300v at $\alpha = 30°$ the peak line-line voltage is $\frac{300}{\cos 30°} \pi/3 \simeq 330V$.

3. Peak forward voltage. The scr may be turned on in the absence of gate drive by exceeding its forward breakdown voltage - this

could be as high as the peak reverse voltage.

4. High dv/dt. A rapid rise of voltage applied between anode and cathode can turn the scr on. This condition exists at turn-on for $\alpha > 0$ and turn off of a valve and is usually absorbed in damping circuits.

5. High di/dt. Circuit conditions which allow the rate of rise of current to be very rapid relative to the scr turn-on time do not exist due to the leakage reactance of the transformer.

With the above considerations taken into account a safety-factor of at least 100% in both current and voltage ratings was allowed. The scr selected was the medium current general purpose scr General Electric C35S rated at 35 Amps and 700 volts.

Each scr was protected by a current limiting fuse [43], which melts extremely rapidly at high current levels but does not interrupt the current too quickly: a high di/dt can induce voltage transients which could damage other scr's. For this reason scr fuses are rated for voltage as well as current, and their total clearing I^2T must not exceed the I^2T [44] factor of the scr.

In addition a damping circuit is provided for each scr to reduce the dv/dt and overshoot of the voltage at scr turn-off. A detailed analysis of valve damping circuits is given in reference [9] and based on those results similar per-unit values for the components of a simple R-C damping circuit were designed and connected in parallel with each scr.

Finally a bypass scr was connected across the terminals of each converter. The bypass valve is used in rectification and, at large values of α, energy from the load, which is normally passed back to the a.c system, bypasses the converter and is returned to the load. The gate of the bypass scr is continuously enabled for rectification and disabled for inversion.

Fig. 3.1 shows the circuit diagram of the converter. The rectifier negative terminal of the converter was used as control ground and a current shunt was connected on this side of the bridge for a current control signal. The isolating switch allows interruption of the rated d.c. current, if necessary.

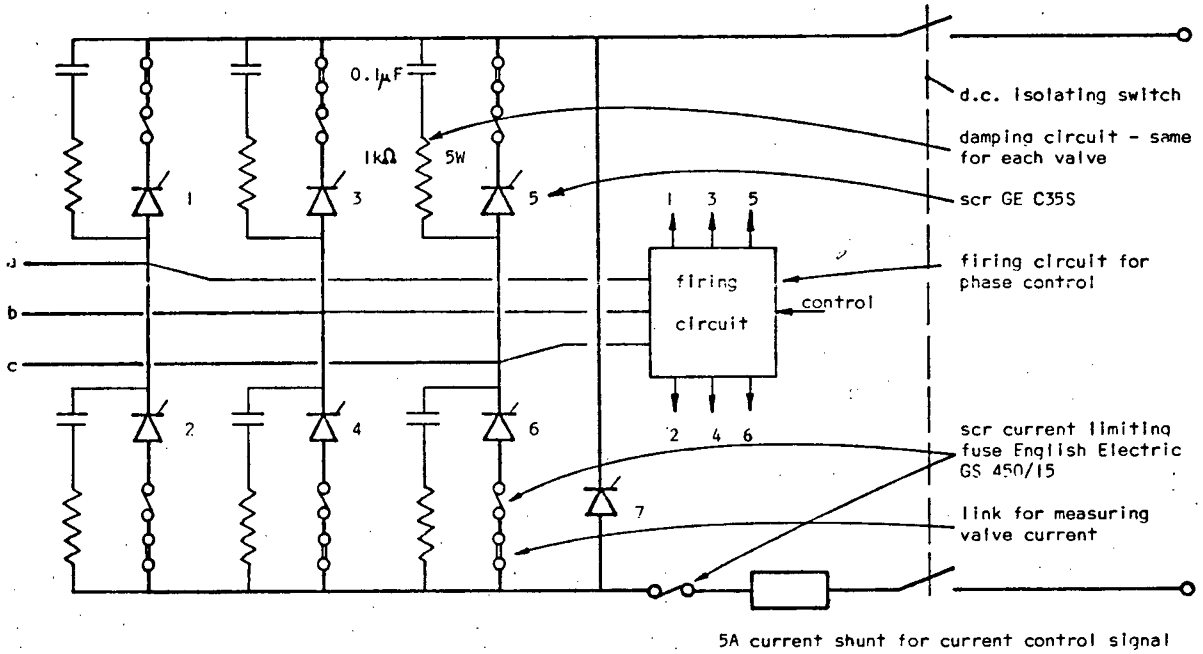

Fig. 3.1 Converter bridge circuit

Each converter was supplied by a power transformer whose function is to isolate the d.c. link from the supply system and provide the necessary voltage control through automatic tap changing. At this stage the on-load tap changer was not built as its use was not anticipated, nor its operation desired in the experimental steady-state stability study. The transformers, rated at 10kVA, custom built by Hammond, incorporate a number of taps for the provision of the tap changer, as in Fig. 3.2. However, since some form of voltage control is necessary to maintain or change an operating point, a three-phase variable autotransformer (variac) was provided at each converter.

The variac also served as additional protection, as acclimatizing experiments could be carried out at relatively low voltages.

The firing circuit required to compute the firing delay was a commercially available 'equal angle' type [see chapter 2.2] consisting of six independent delay elements which operate according to the magnetic amplifier principle of delaying the saturation of a saturable core by a d.c. control current: at the instant of saturation the sudden change in permeability of the core reduces the back emf in the exciting coil, resulting in a sudden increase of current in the excitation circuit . After a further process of shaping this pulse is delivered to the gate of the appropriate scr.

The firing circuit required a three phase 240v input for excitation. Since the local supply was 208 volts the required voltage was conveniently obtained using the combination of transformer windings shown in Fig. 3.2 obviating the use of a separate transformer.

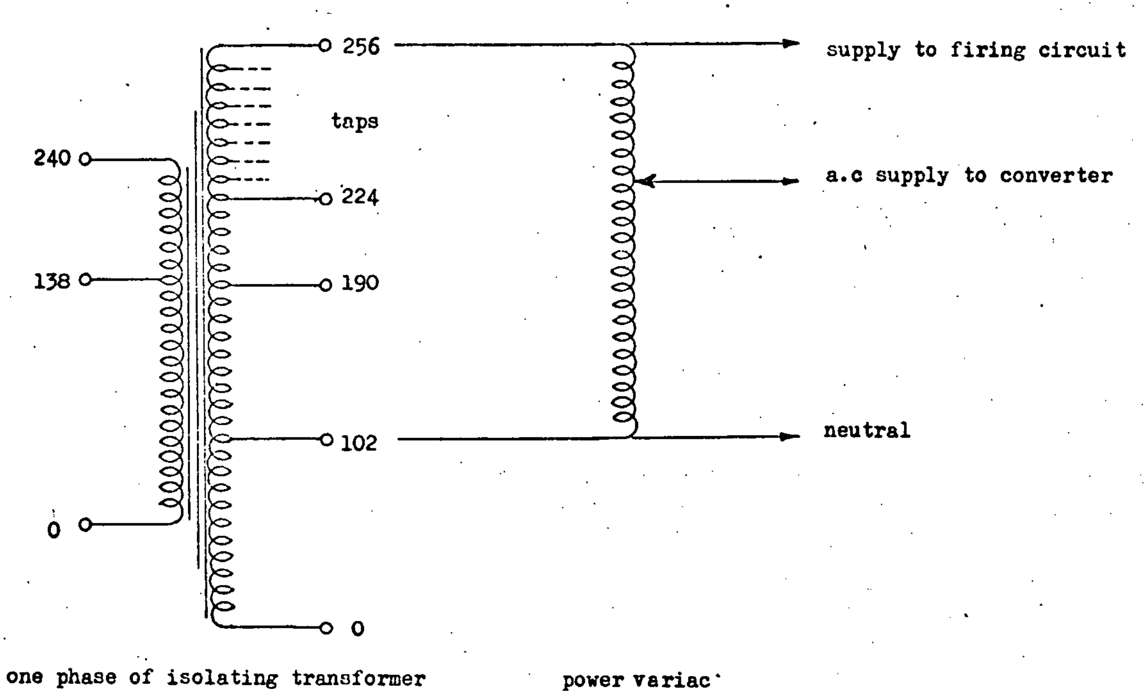

Fig 3.2 Single Phase Diagram of Transformer and Variac Connections

3.2 Mathematical Representation

In the steady state analysis of high voltage converters the following assumptions are usually made[28,29]:

(i) The a.c input voltage is assumed to be sinusoidal and balanced in both amplitude and phase. Only fundamental quantities of voltage and current are considered.

(ii) The effect of d.c. ripple is neglected: this assumes the presence of a perfect filter, usually characterized by a smoothing choke of infinite inductance and zero resistance placed at the terminals of the converter.

(iii) The resistance of the transformer and a.c. system are negligible.

(iv) The valves are assumed to be perfect circuit elements:

the forward voltage drop of a conducting valve and the reverse leakage current while blocking are both considered negligible.

The equations presented here describe the voltage and current relationships of the two terminal d.c. link shown in Fig. 2.6. These equations are used to determine system parameters such as commutating reactance, overall effective firing angle. The steady state equations are presented here without derivation, which may be found in any standard text [10]. In the following equations the 'r' and 'i' subscripts denote rectifier and inverter quantities respectively.

The voltage equation for the rectifier is given by

$$V_{dr} = \frac{1}{2}V_{dor}[\cos\alpha + \cos(\alpha + u_r)] \tag{3.1}$$

where V_d = converter direct output voltage

V_{do} = converter 'no-load' voltage with zero firing delay

α = firing angle, measured from earliest possible instant that valve could conduct.

u_r = the angle of commutation.

The current equation of a rectifier is given by

$$\frac{3}{\pi}X_{cr}I_d = \frac{1}{2}V_{dor}\ [\cos\alpha - \cos(\alpha + u_r)] \tag{3.2}$$

where I_d is the d.c. line current

X_{cr} is the commutating reactance per phase

Addition of equations (3.1) and (3.2) yield the more popular version of the converter voltage equation:

$$V_{dr} = V_{dor}\cos\alpha - \frac{3}{\pi}X_{cr}I_d \qquad (3.3)$$

The two corresponding equations for the inverter are

$$V_{di} = \frac{1}{2}V_{doi}[\cos(\beta - u_i) + \cos\beta] \qquad (3.4)$$

$$\frac{3}{\pi}X_{ci}I_d = \frac{1}{2}V_{doi}[\cos(\beta - u_i) - \cos\beta] \qquad (3.5)$$

whence $$V_{di} = V_{doi}\cos\beta + \frac{3}{\pi}X_cI_d \qquad (3.6)$$

Alternatively, since $\delta = \beta - u_i$ these equations may be written

$$V_{di} = \frac{1}{2}V_{doi}[\cos\delta + \cos\beta] \qquad (3.7)$$

$$\frac{3}{\pi}X_{ci}I_d = \frac{1}{2}V_{doi}[\cos\delta - \cos\beta] \qquad (3.8)$$

$$V_{di} = V_{doi}\cos \quad - \frac{3}{}X_{ci}I_d \qquad (3.9)$$

The d.c. line current is determined from the difference in direct voltage at each end of the line.

$$I_d = \frac{V_{dr} - V_{di}}{R_{dc}} \qquad (3.10)$$

Where R_{dc} is the resistance of the d.c. line. In practice the inductance smoothing choke is finite but the effect of ripple is still neglected. The current equation (3.10) becomes more accurately, in transformed form

$$I_d = \frac{V_{dr} - V_{di}}{R_{dc} + sL_{sm}} \qquad (3.11)$$

where L_{sm} is the value of inductance of the smoothing choke.

Neglecting losses in the converter, the total a.c. real power input is equal to the d.c. power output

rectifier: $$3I_1V_1\cos\phi_1 = V_{dr}I_d \qquad (3.12)$$

$$\text{inverter:} \qquad 3I_2V_2 \cos\phi_2 = V_{di}\, I_d \tag{3.13}$$

where V and I are the fundamental voltage and current phasors. The phase angle between them is given by Read[35]

$$\tan\phi = \frac{u - \sin(u)\,\cos(2\alpha + u)}{\sin(u)\,\sin(2\alpha + u)} \tag{3.14}$$

However the following more convenient approximate formula is used[11]: the error incurred from using the approximation is shown in Fig. 3.5

$$\cos\phi_1 = \frac{1}{2}\,[\cos\alpha + \cos(\alpha + u_r)] \tag{3.15}$$

$$\cos\phi_2 = \frac{1}{2}\,[\cos\beta + \cos\,\delta] \tag{3.16}$$

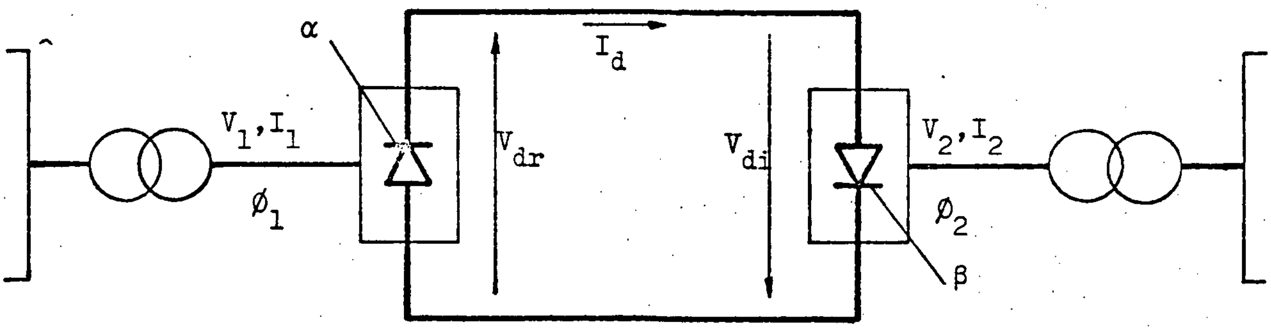

Fig 3.3 A.c. and d.c. Quantities in the Link

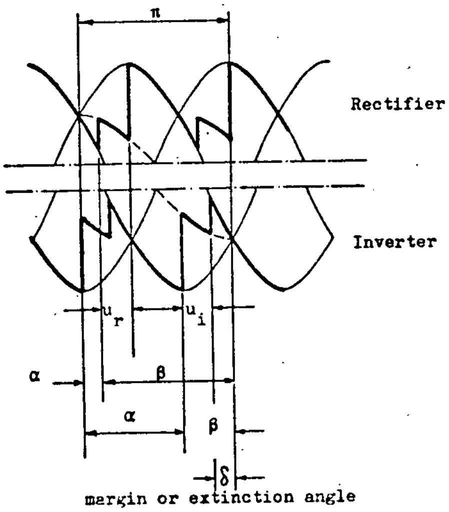

Fig 3.4 Rectifier and Inverter Angles

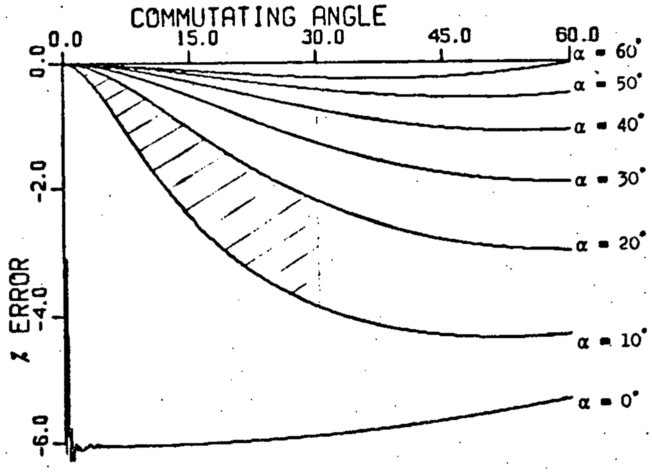

Fig 3.5 Error incurred in using the Approximate Formula for Phase Angle on a.c. side of Converter

3.3 Initial Experimental Testing

The firing circuits

The firing circuits were manufactured by Firing Circuits Inc., Model 613A372. Connection of the firing circuit to the scr converter as per manufacturer's instructions [46] resulted in the following disposition of firing angle pulse and a-c phase voltage, Fig. 3.6(a).

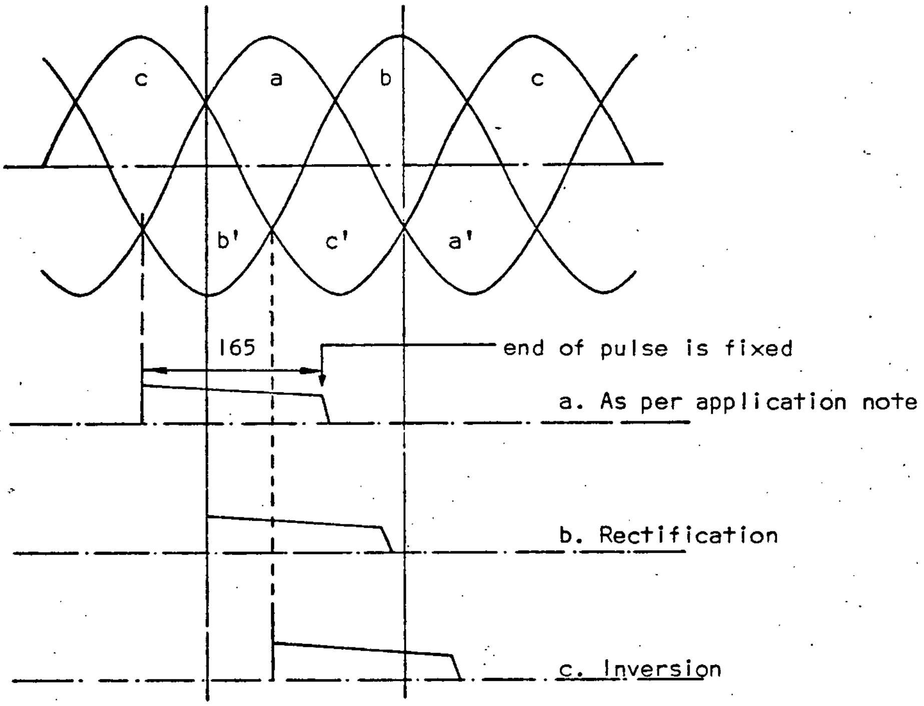

Fig 3.6 Phase Voltage and Firing Pulse for SCR I

where it can be seen that 60° of phase control is not used. A more efficient use of the firing pulse is shown in Fig 3.6(b) where the pulse specified for valve 6 is used to trigger valve 1. Since the end-of-pulse is fixed, the maximum range of 165° does not allow the continuous transition from rectification to inversion. The full range of the inverter is possible by using the pulse specified for valve 3 to trigger valve 1. The modified connection table is shown in Table 3.7.

Firing Circuit gate number [46]	used to fire scr no.	
	Rectification	Inversion
1	4	5
2	3	6
3	6	1
4	5	2
5	2	3
6	1	4

Table 3.7 Modified Connections

The firing circuits were provided with 4 control windings of 100, 200, 500, 1000 Turns. The amplifiers used to construct the control system and drive the firing circuit were those comprising The DONNER Analog Computer. Due to saturation of these amplifiers only the two low current windings [500T, 1000T] provided control over the total possible range. Also, a resistor connected in series with each control winding increased the speed of response specified[46] as $0.004[\frac{N^2}{RWDG + R}] + 12$ m sec.

Although the firing circuit is essentially a current controlled device, it is more convenient for the purposes of analysis to measure transfer functions as ratios of two voltages or radians to voltage. Thus the control voltage-firing angle characteristics are shown in Figs. 3.8(a) and (b) for rectification and inversion respectively for each firing circuit according to the modified connection.

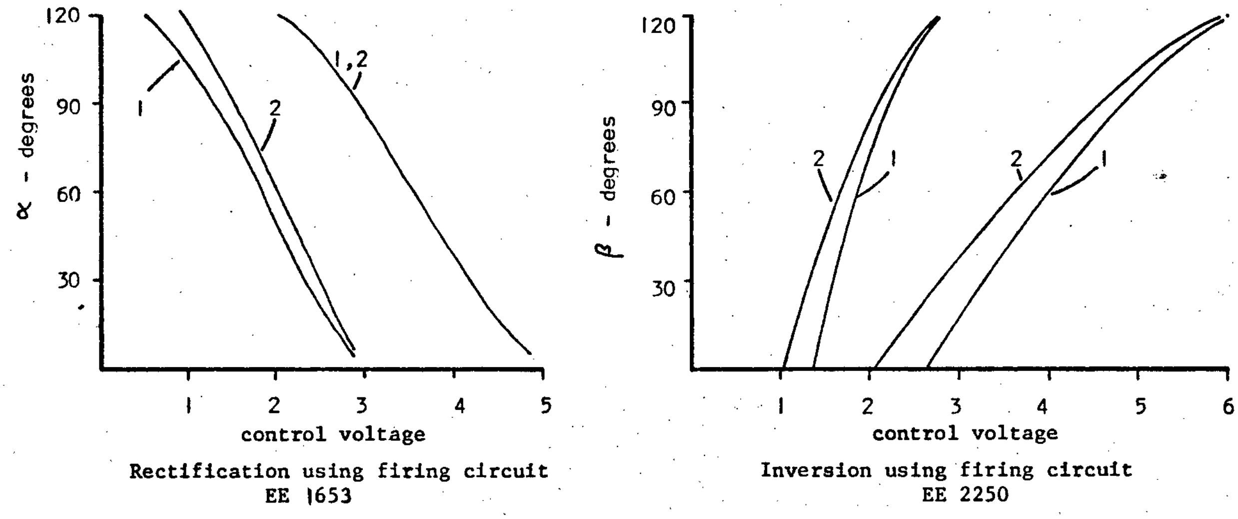

Fig 3.8 Control Voltage - Firing Angle Characteristics

Within the typical operating range of α[10° - 30°] and β[15° - 50°] the firing circuits are linear. The incremental gains for each low-current winding are shown in table 3.9.

Firing Circuit	Rectification		Inversion	
	1000T	500T	1000T	500T
1	0.69	0.37	1.5	0.32
2	0.69	0.43	1.25	0.21

Table 3.9 Incremental Gains shown in Radians per Volt

The frequency response of the firing circuit was measured using the arrangement show in Fig. 3.10.

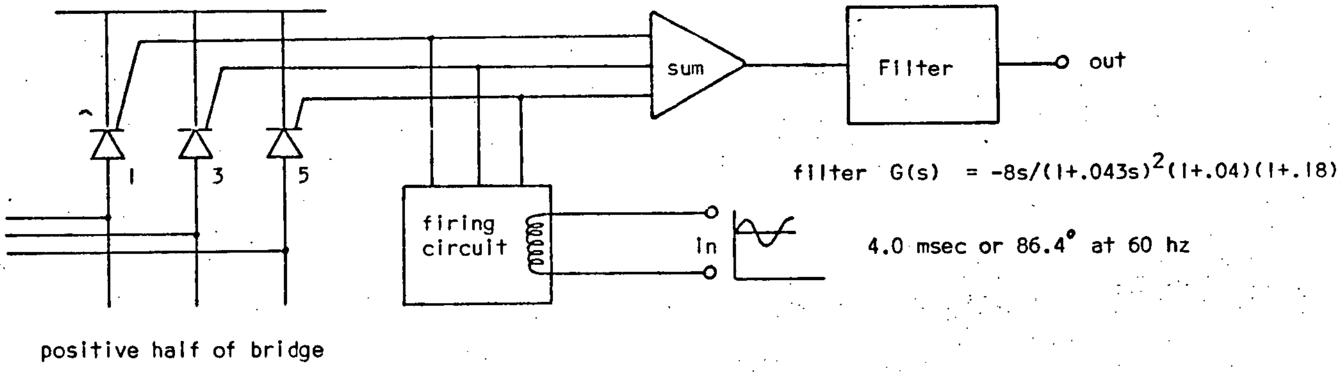

Fig 3.10 Measurement of Frequency Response

The input frequency was varied from 1 to 40hz and the amplitude and relative phase of the output was measured. From the overall response was subtracted the measured frequency response of the filter, resulting in the following amplitude and phase plot.

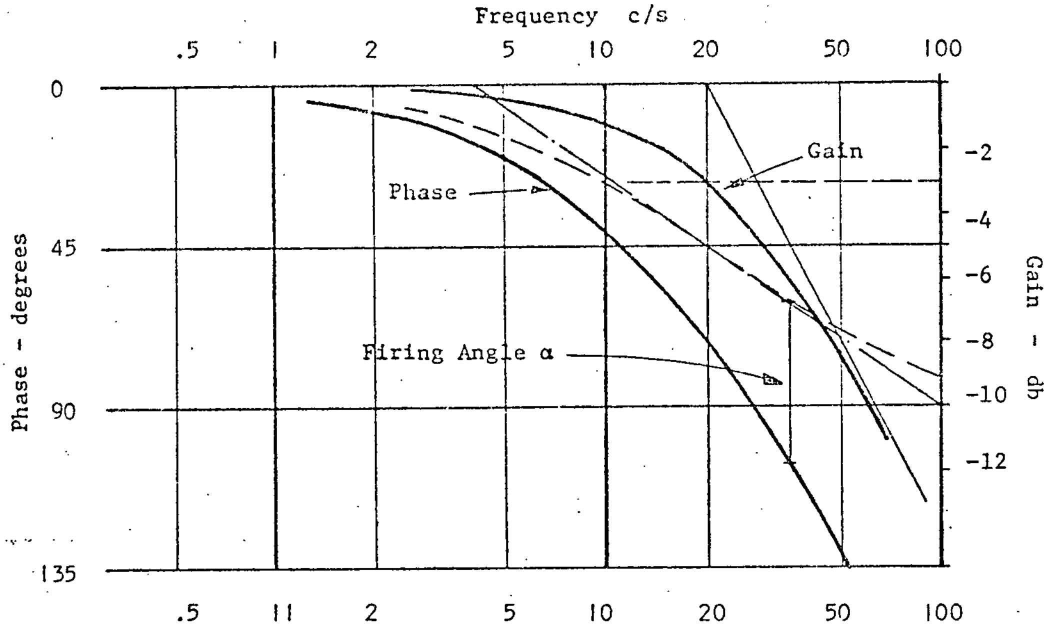

Fig 3.11 Firing Circuit Frequency Response - 500T Winding

With the gain falling off at 6db/octave a 1st order element is suggested, but the phase falls off to well beyond 90°. By subtracting the firing angle of 4 m sec from the phase characteristic, a well behaved 1st order linear element appears. This suggests a transfer function of $F(s) = \frac{G}{1+0.008s}$ with a transport lag which will be neglected for low-bandwidth systems but otherwise equal to the firing curcuit delay angle:

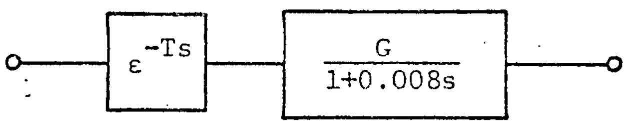

$T = \frac{\alpha}{2\pi.60}$ for rectifier

$T = \frac{\pi/3 - \beta}{2\pi.60}$ for inverter

G = incremental d.c. gain - see Table 3.9

Fig 3.12 Block Diagram of Firing Circuit

The measurements made were estimated to be within $\pm$ 10% error, and within this margin, both firing circuits were estimated to have the same frequency response for the 500T winding.

Two other effects: the firing angle changes with applied a.c.voltage, and due to distortion caused by the voltage dents which appear at commutation a relation between the current and the change in firing angle may be measured, Fig 3.12. Fig. 3.13 shows the change in α at different values of α for changes in a-c voltage (undistorted).

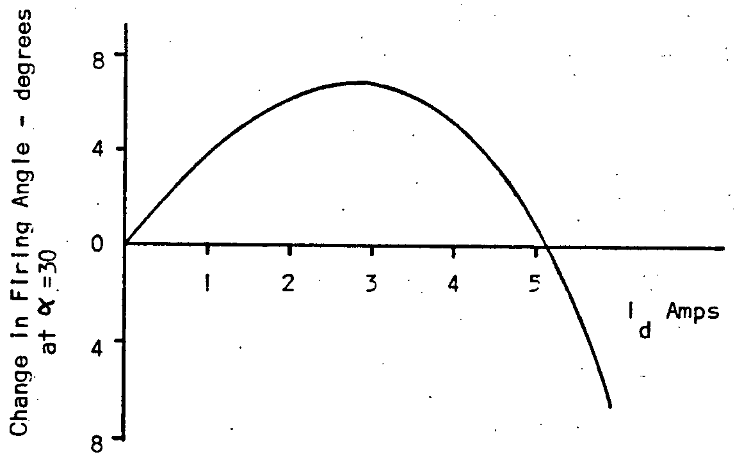

Fig 3.13 Typical Variation of firing angle with change in current

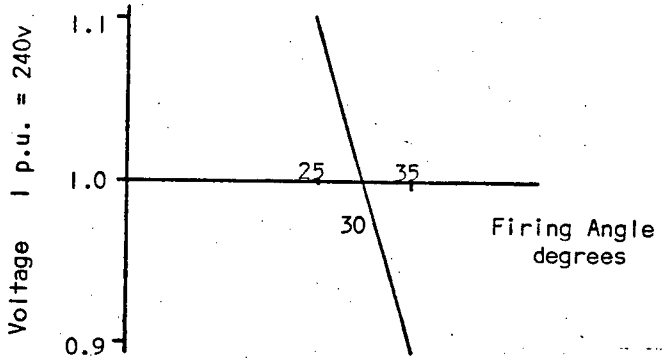

Fig 3.14 Typical Variation of firing angle with phase voltage input to firing circuit

Measurement of Transformer commutating reactance

The leakage reactance of the transformer was measured by operating the rectifier with a resistive load. Application of equation (3.2) yields a value of commutating reactance of 0.03 Ω/phase.

The commutating reactance may be increased by the insertion of additional external reactance, which may be placed on either side of the variac, Fig. 3.15.

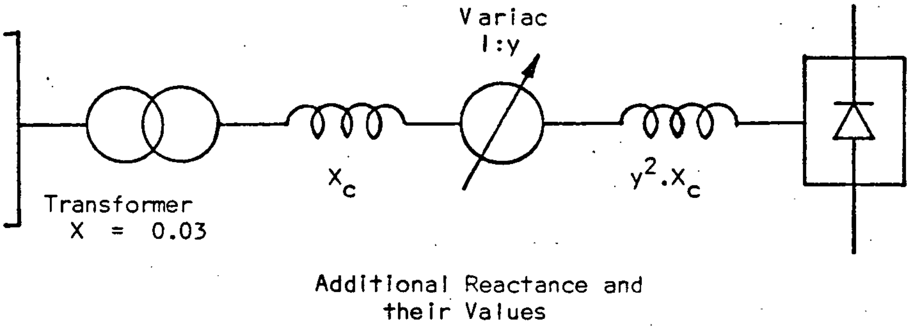

Fig 3.15 Insertion of Additional Commutating Reactance

Inductors of nominal values 5, 10, 20 mH are available, each found to have a reactance of 1.4, 5, 9 ohms respectively and negligible resistance.

3.4 D.C. Link Start-up Procedure

In energizing the link, the essential precaution is to first set the voltage at the inverter to the nominal operating voltage using the inverter variac and with the inverter firing circuit delivering pulses at around $\beta = 25°$. Then the rectifier is brought up to the operating voltage so that the link current starts from zero. The final operating point - desired V_{dr}, V_{di}, I_d, α, β - is achieved through adjustments in variacs and firing circuit controls.

A change in operating voltage upwards is initiated with adjustment of the inverter variac, a change in voltage downwards is initiated with adjustment of the rectifier variac, tending to keep the current low. And, in the absence of the inverter feedback control, the extinction angle is carefully monitored and adjusted if it falls below 15°.

Model users are advised to acclimatize to this procedure using low voltage and current levels.

This chapter has presented the basic components of the physical model and their mathematical behaviour. The omission of filters was not regarded as detrimental to the realism of the model since no satisfactory model a.c.system exists for their behaviour [voltage regulation at the converter's a.c. terminals] to be appreciated. Instead the converters were operated using the local hydro system which easily accommodated the reactive power requirements of the converters.

The following chapters describe the converter control systems with attendant studies in relative stability. The inverter control is developed first as a protective measure.

4. INVERTER CONTROL

The controlled operation of the d.c. link requires regulation at both rectifier and inverter. Although the link may be operated with both stations on open loop, the risk is great of commutation failure at the inverter, resulting in excessively large currents. Operation at a large enough angle of β at the inverter also results in a large component of reactive power.

Hence the first priority is the prevention of inverter commutation failure i.e. constant extinction angle control. This chapter describes the realization of the inverter control characteristic shown in Fig. 2.7. The first section describes in detail the principles of inverter c.e.a. control; the second a new method of detection of extinction angle; the third section describes the physical components of the control system and the fourth section derives the mathematical model in the form of the characteristic equation.

4.1 General Principles of Operation

The constant extinction angle control is important to the inverter station in that it protects the inverter from commutation failure by advancing the firing angle β in response to a decrease in margin or extinction angle δ, see Fig. 4.1. The inverter normally operates on a characteristic which keeps the margin angle constant at its lowest safe value to minimize reactive power demand. The margin angle δ is maintained typically

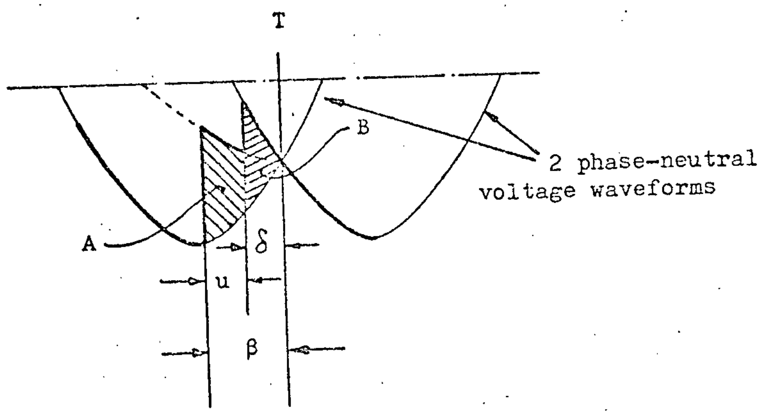

Fig 4.1 Inverter Commutation

at 15-20°[47] to allow for valve de-ionization and control system inaccuracies before the commutation voltage turns negative after which it becomes impossible to initiate or complete successful commutation.

Given that the extinction angle is required to remain constant, the problem is to anticipate the duration of the commutation period, since, once the valve is triggered, there is no control over the resulting extinction angle, which becomes critical. The 'in-coming' valve must reach full conduction in order to turn off the 'out-going' valve. If commutation is not complete by instant 'T' in Fig. 4.1, the current will start to commutate back to the original valve, resulting in commutation failure, excessive d.c. line current and possible damage if there is no means of recovery. The inverter controller, therefore, must respond to changes in current and extinction angle to produce the required angle of advance β. For this reason, the c.e.a. control is referred to in some literature as predictive.

There are two basic approaches to the implementation of c.e.a. control: the first is called the "angle comparator method",[41,48] where comparison of control signals proportional to δ and u with the desired reference extinction angle effects adjustment of angle of advance β. The second approach is called the "volt-integral comparator method",[47,49,14] where the control signals are proportional to the volt-time areas associated with commutation and after extinction, areas 'B' and 'A' respectively in Fig. 4.1. In these reported cases [37,42,47,48,49] the firing angle β is computed from predicted (or known from last firing) values of u and β and devices were developed to detect u and δ separately.

The next section describes a simple method, devised by the author, detecting the extinction angle of each valve directly, without the need for detecting two angles separately. The output of the detector is a pulse of equal duration to the extinction period, which may then be used in either of the two approaches mentioned above.

4.2 A New Method of Detection of Extinction Angle

The method consists of comparing the direct voltage of the inverter with the output of a diode 3-phase bridge circuit connected to the same secondary winding of the inverter transformer. This results in an interesting compensation for the commutation voltage drop due to the transformer leakage reactance.

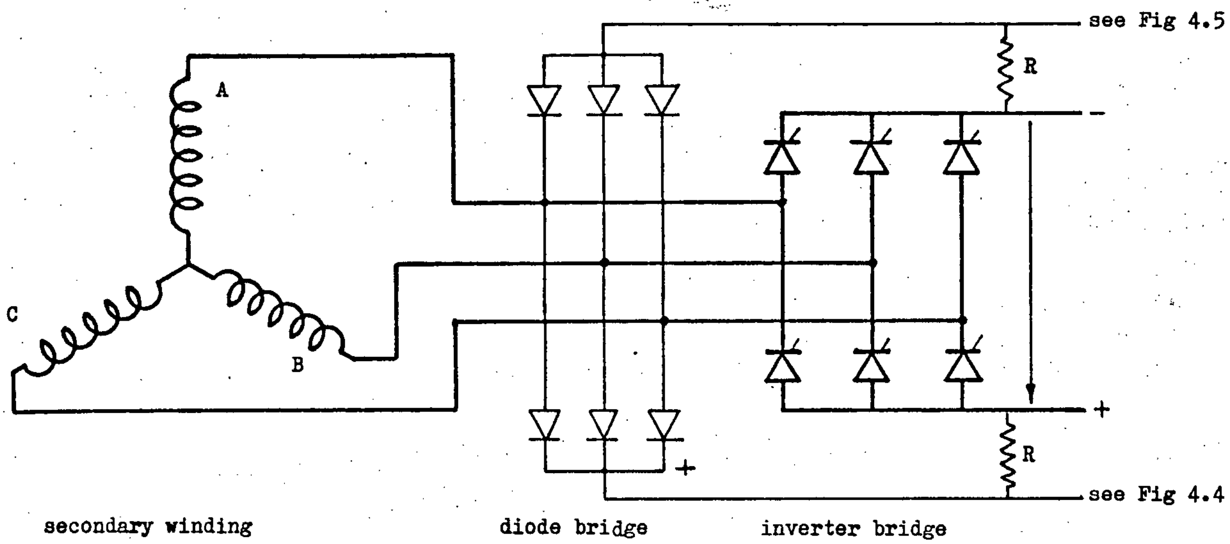

Fig 4.2 Inverter Extinction Angle Detector

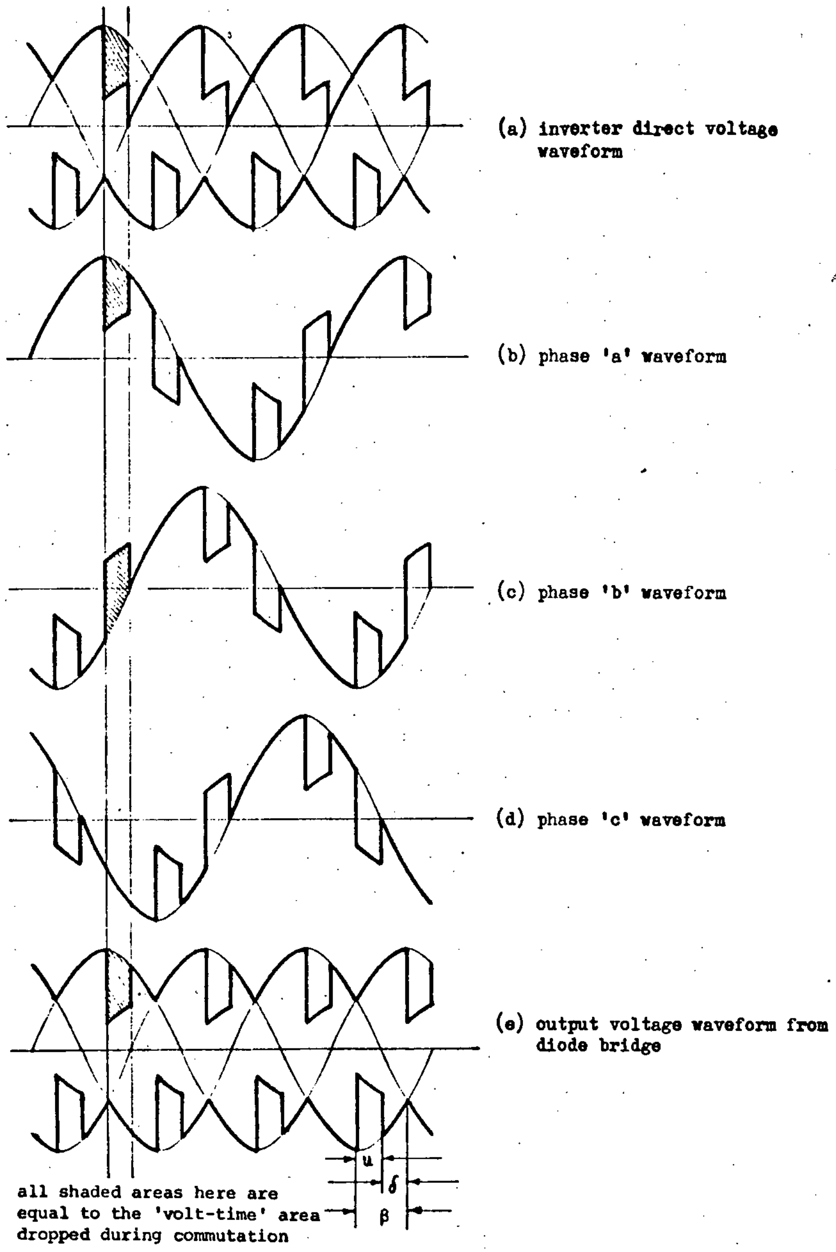

Fig 4.3 Distortion of a.c. Waveforms by Inverter Commutation and Effect on Diode Bridge Output

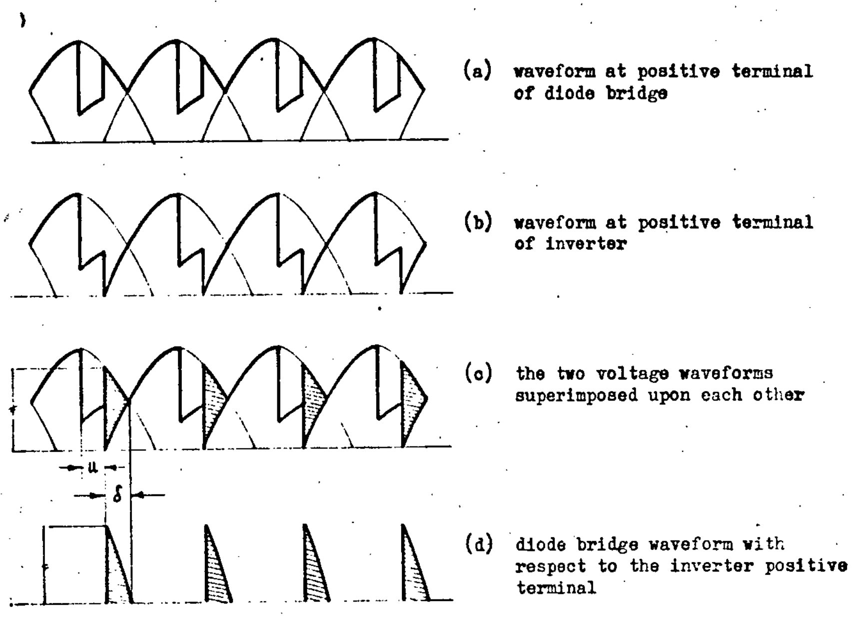

Fig 4.4 Pulse Waveform Produced by Subtraction of Inverter Waveform from Diode Bridge Waveform, shown for the Positive side of the Inverter

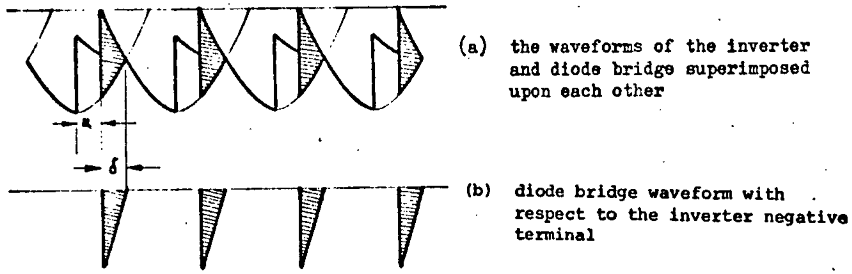

Fig 4.5 Pulse Waveform on the Negative Side of the Inverter

The detector circuit, shown in Fig. 4.2 consists of a three-phase diode bridge which produces a rectified voltage waveform with no phase control. It is connected to the inverter, with similar polarities connected, via resistors R, which enable current to flow through the diode bridge.

The effective short circuit between two phases during commutation results in the impression of 'voltage dents', as shown in Fig. 4.3(b-d). If these same phase voltages supply the diode bridge, rectified output has a waveform similar to that shown in Fig. 4.3(e). The 'dent' in each pulse of the diode output waveform has the same volt-time area as the inverter commutation volt-drop.

By monitoring the voltage on each side of the diode bridge with respect to the voltages on each side of the inverter, the two voltages are effectively subtracted. The result is two trains of pulses, shown in Fig. 4.4(d) for the voltage positive side of the bridge, and Fig. 4.5(d) for the negative side of the bridge. Each pulse has an angular duration identical to the extinction angle, amplitude equal to the instantaneous value of commutating voltage at extinction, and volt-time area equal to the volt-time area left after extinction of each valve to the end of positive commutating voltage.

In the model, the positive pole of the inverter was taken as control ground, and the pulses shown in Fig. 4.5(b) were exclusively used. The application of the detector to the inverter c.e.a. control system is described in the next section.

4.3 Implementation of the Inverter Control Characteristic

The inverter control characteristic, shown in Fig. 2.7, is reproduced in Fig. 4.6: normal operation is with c.e.a. control, but a constant current control is usually included to prevent a break in transmission should the rectifier voltage fall.

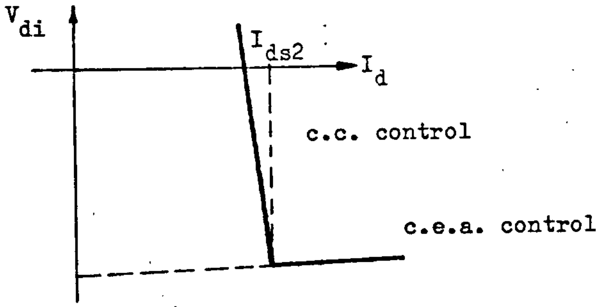

Fig 4.6 Inverter Control Characteristic

Constant Extinction Angle Control

A feedback control is apparent where one of the two trains of margin angle pulses is low-pass filtered and compared to a reference to produce an error signal, amplified by the error amplifier to drive the firing circuit. The d.c. output of the low-pass filter is proportional to the average volt-time area of the pulses, related to the margin angle, as in Fig. 4.7, by

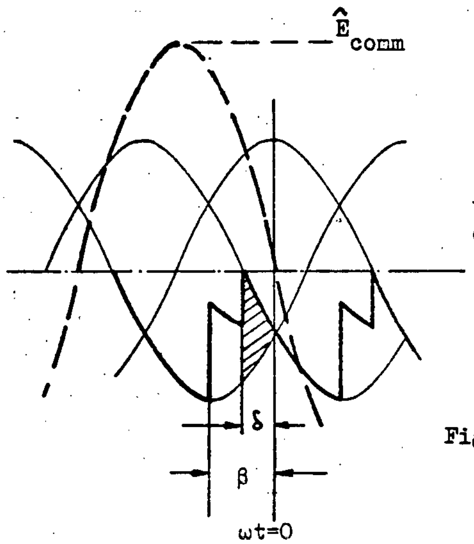

Fig 4.7

$$V_{ave} = 3.\frac{1}{2\pi} \int_{-8}^{\circ} - \hat{E}_{comm} \sin(\omega t).d(\omega t)$$

$$= \frac{3}{2\pi} \hat{E}_{comm} [1 - \cos\delta]$$

$$= \frac{1}{2}V_{doi} [1 - \cos\delta] \quad \text{i.e. non linear}$$

And for small changes in δ about an operating point

$$\Delta V_{ave} = [\frac{1}{2} \Delta V_{doi} (1 - \cos\delta) + \frac{1}{2} V_{doi} \sin\delta\Delta S] F(s)$$

also nonlinear, and where F(s) is the transfer function of the filter. This non-linearity may be avoided by the addition of a zener diode, Fig. 4.7, whence $V_{ave} \propto \delta$.

Although the diode switch-off produces a definite slope, and due to balance error, each pulse has a different duration, linearity over the whole operating range of β was found ($\beta \geq 10°$). From practical experience it was found that the filter was unnecessary, and in the case of a single pole filter, contributed to a potentially undesirable transient overshoot response to a step change in margin.

Since c.e.a. control is essentially predictive in nature, and since its function in maintaining minimum safe margin angle for inverter protection, an additional feature to the c.e.a. controller would be an asymmetric response to positive and negative d-c current transients: in response to an increase in current, and hence an increase in commutation angle and a decrease in margin angle, a fast control action to increase β is desirable. Momentary overshoot could be tolerated Fig. 4.8(a), so long as the time constant of its decay was smaller than the time constant provided by the smoothing choke in governing the rate of increase of line current. However, in response to a decrease in current, little or no overshoot is required, rather a slow critically damped response, Fig. 4.8(b). Such a feature is described at the end of the chapter, but not included for analysis.

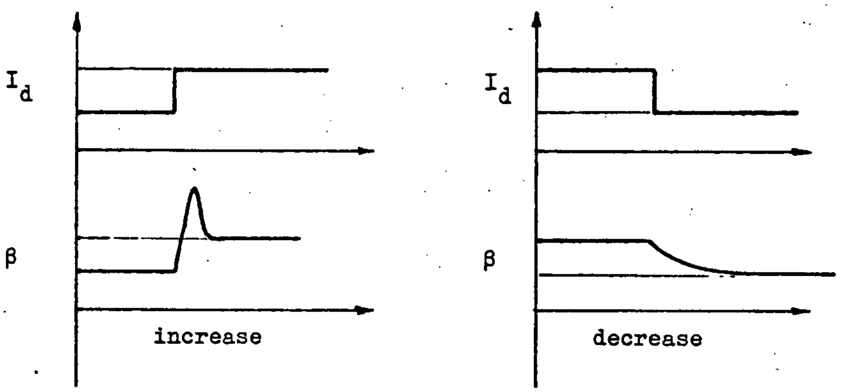

Fig 4.8 C.E.A. Controller Responses to Increases and Decreases in Current

Constant Current Control

Inverter operation requires that, when the current falls below a certain value, the control mode changes to maintain constant current control, which is normally 20% below the constant current setting of the rectifier. This is achieved in the model by providing additional error signal when the current falls below the current setting I_{ds2}, shown in Fig. 4.9.

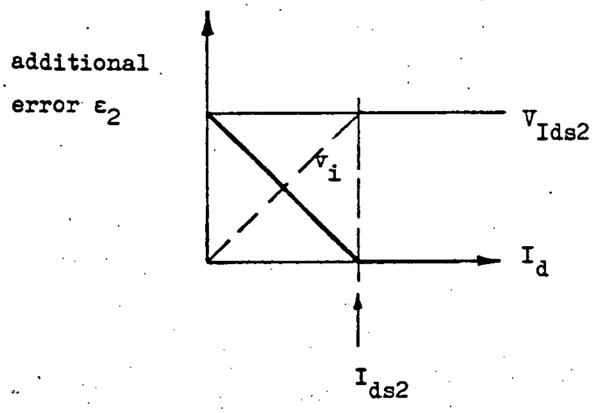

Fig 4.9
Additional Error Signal when $I < I_{ds2}$

The current signal proportional to current below I_{ds2} and then damped to $V_{I_{ds2}}$ when $I_d > I_{ds2}$: subtraction of this signal from the reference $V_{I_{ds2}}$ gives an additional error signal proportional to $(I_{ds2} - I_d)$. The overall model control system is shown in Fig. 4.10.

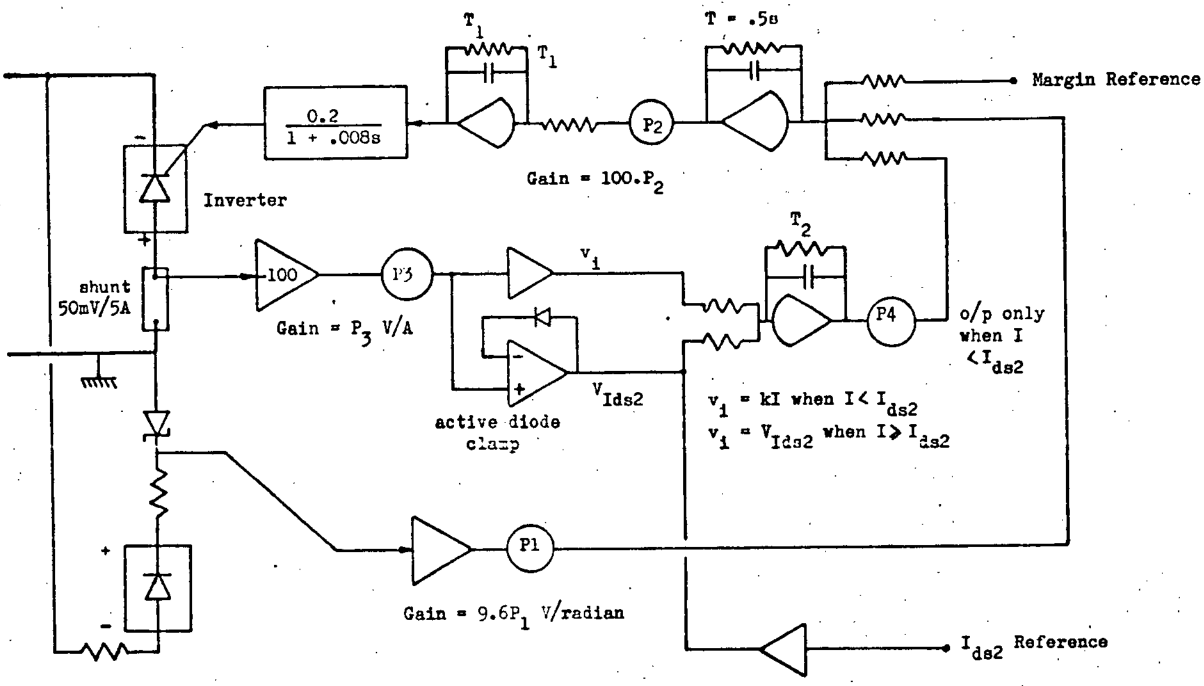

Fig 4.10 Constant Extinction Angle and Constant Current Controls for Inverter

4.4 Mathematical Models

This section derives the mathematical model in the form of the linearized perturbed equations. As outlined in the introduction, the equations are written down to describe the practical system: an operating point was established, the feedback loop introduced and the details of the operating point form the basis of the perturbed equations. As usual the Laplace transform is used.

The characteristic equation is derived for both the c.e.a. and c.c. control for the inverter which was supplied by a power supply, and not the rectifier. From the system equations written in matrix form the characteristic equation is derived as the determinant of the coefficient matrix using an efficient computer program employing a novel method illustrated in Appendix A.

For the application of Siljak's method, described in chapter 5, two adjustable parameters were chosen arbitrarily as two parameters of the error amplifier.

The inverter was operated such that a small disturbance did not result in a change in control mode from c.e.a. to c.c. or vice versa.

Constant Extinction Angle Control

The block diagram for c.e.a. control, derived from the circuit shown in Fig 4.10, is shown in Fig. 4.11. The G_2 block arises from the interference with firing angle by changes of d.c. line current through distortion of the a.c. line voltage - see Fig. 3.13. A numerical constant has been assigned to G_2, even though a small time constant probably exists.

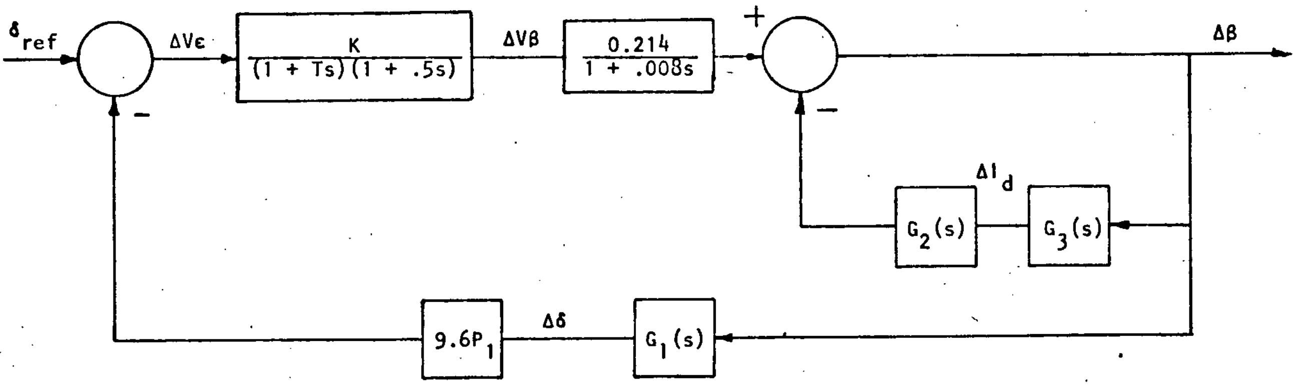

Fig 4.11 Block Diagram of c.e.a. Controller

In response to a small disturbance, the linearized Laplace transformed equations may be written:

$$\Delta V\varepsilon = -9.6P_1 \ \Delta\delta \tag{4.1}$$

where P_1 is the actual setting of the potentiometer P_1 in the c.e.a. feedback loop of Fig. 4.10

$$\Delta V\beta = \frac{K}{(1 + Ts)(1 + 0.5s)} \ \Delta V\varepsilon \tag{4.2}$$

where K and T are two arbitrary adjustable parameters used in Siljak's analysis.

$$\Delta\beta = \frac{0.214}{1 + 0.008s} \ \Delta V\beta - G_2(s)\Delta I_d \tag{4.3}$$

using the 500-turn control winding, and G_2 measured at the operating point. An expression for $G_1(s)$ relating $\Delta\beta$ and $\Delta\delta$ may be derived from the following power equations

$$V_{di} = \frac{1}{2} V_{dio} \{\cos\delta + \cos\beta\} \tag{4.4}$$

$$\frac{3}{\pi}X_c I_d = \frac{1}{2} V_{dio} \{\cos\delta - \cos\beta\} \tag{4.5}$$

$$I_d(R_{dc} + sL_{sm}) = V_{dr} - V_{di} \tag{4.6}$$

With the available d.c. power supply driving the inverter, V_{dr} is assumed constant, and with the inverter feeding into a large a.c. system, and without regulation provided by filters, V_{doi}, related to the a.c. system voltage, is also assumed constant. The linearized perturbated equations become

$$\Delta V_{di} = -\frac{1}{2}V_{dio}\sin\delta\;\Delta\delta - \frac{1}{2}V_{dio}\sin\beta\;\Delta\beta \tag{4.7}$$

$$\frac{3}{\pi}X_c\;\Delta I_d = -\frac{1}{2}V_{dio}\sin\delta\;\Delta\delta + \frac{1}{2}V_{dio}\sin\beta\;\Delta\beta \tag{4.8}$$

$$\Delta V_{di} = \Delta I_d\;(R_{dc} + sL_{sm}) \tag{4.9}$$

from which
$$G_1(s) = \frac{R_{dc} + X_c + sL_{sm}}{R_{dc} - X_c + sL_{sm}} \tag{4.10}$$

as in
$$\Delta\delta = G_1(s)\;\Delta\beta \tag{4.11}$$

Similarly, an expression for $G_3(s)$, relating ΔI_d and $\Delta\beta$, may be derived from equations (4.7-9). However the approach used in this study was to write down the relevant equations in matrix form and compute the determinant by a method developed by the author in conjunction with Dr. Kabriel [52] [see Appendix A]. In this case the relevant equations are (4.1-3), (4.7-9) and, written in matrix form, appear as

$$\begin{array}{cccccc}
\Delta V_\varepsilon & \Delta V_\beta & \Delta\beta & \Delta\delta & \Delta V_{di} & \Delta I_d \\
\end{array}$$

$$\begin{bmatrix}
1 & & & 9.6P_1 & & \\
-K & (1+Ts)(1+0.5s) & & & & \\
 & -0.214 & 1+0.008s & & & k_2(1+0.008s) \\
 & & \frac{1}{2}V_{dio}\sin\beta & \frac{1}{2}V_{dio}\sin\delta & 1 & \\
 & & -\frac{1}{2}V_{dio}\sin\beta & \frac{1}{2}V_{dio}\sin\delta & & 3X_c/\pi \\
 & & & & 1 & R_{dc}+sL_{sm}
\end{bmatrix}
\begin{bmatrix}
\Delta V_\varepsilon \\ \Delta V_\beta \\ \Delta\beta \\ \Delta\delta \\ \Delta V_{di} \\ \Delta I_d
\end{bmatrix} = 0$$

A computer program, primarily intended for larger sparse matrices, was used to compute the determinant, where some elements are to be retained as algebraic variables and some are polynomials in s. The program utilizes efficient sparse matrix methods. The determinant of the coefficient matrix is known to be the characteristic equation of the system. Hence

$$\Delta(s) = \sum_{k=0}^{n} a_k s^k = 0 \tag{4.13}$$

is the characteristic equation governing the description of system behaviour following a small disturbance from a steady operating point.

The inverter and its control was operated alone using a d.c. power supply. In doing so, the full range of inverter behaviour may be investigated without interference from the rectifier control system.

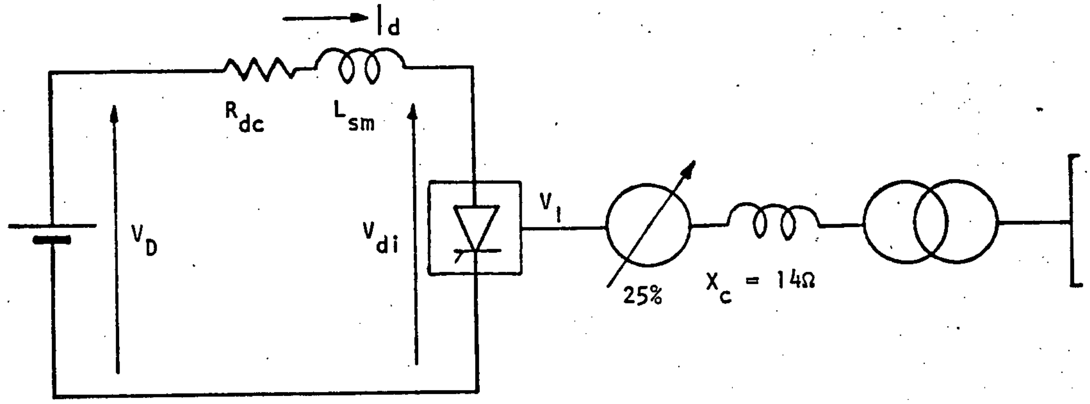

Fig 4.12 Inverter Operating Point

V_d = 109v	V_{di} = 88v	V_I = 40v	hence V_{dio} = 98v
I_D = 5.0A	R_{dc} = 4.1Ω	L_{sm} = 1.2H	X_c = 14(0.25) = 0.88Ω
δ = 19.5°	β = 31.0°		

For $I_{BASE} = 5A$ $V_{BASE} = 100v$, the coefficient matrix becomes

$\Delta V\varepsilon$	$\Delta V\beta$	$\Delta\beta$	$\Delta\delta$	ΔI_d	ΔV_{dio}
1.			6.3		
-K	$1+(0.5+T)s+0.5Ts^2$				
	-0.214	1+0.008s			0.2+0.0016s
		0.252	0.165	1.	
		-0.252	0.165		0.044
				1.	0.205+0.06s

the determinant of which is

$$\begin{aligned} 0 = {} & 5.77 + 5.47K \\ & +(3.92 + 2.04K + 5.77T)s \\ & +(0.526 + 3.92T)s^2 \\ & +(0.004 + 0.526T)s^3 \\ & + 0.004Ts^4 \end{aligned} \tag{4.14}$$

and this is the characteristic equation for the c.e.a. controller. The next chapter describes the application of Siljak's method to the characteristic equation in this form.

Constant current control

The constant current controller is activated when the operating current falls to the current corresponding to the reference setting I_{ds2} in this case set at 7A. The block diagram for the constant current control is shown in Fig. 4.13.

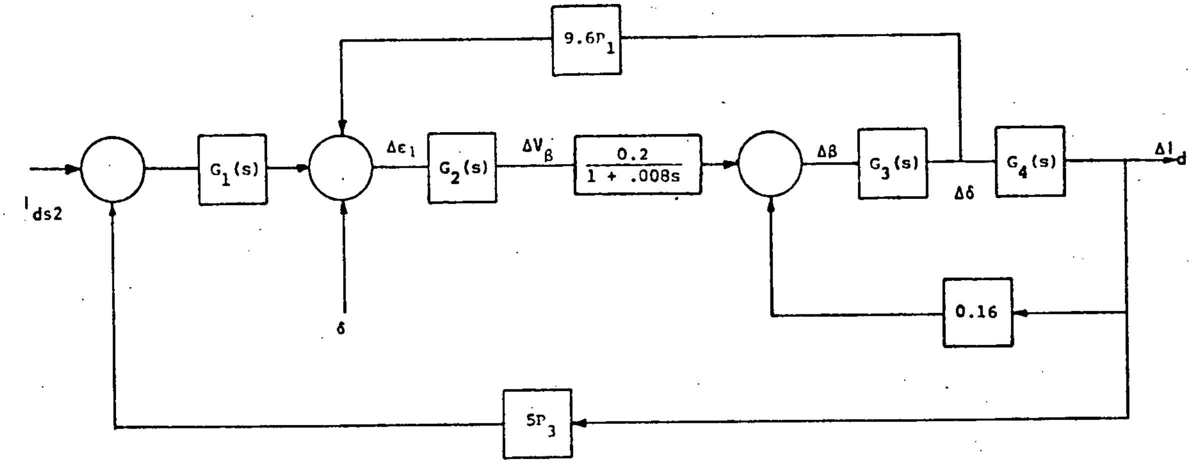

Fig 4.13 Block Diagram for Inverter Constant Current Control Mode

The constant current feedback loop produces an error signal which tends to increase β when the current falls: the increase in β is accompanied by an increase in δ which tends to cause a reduction in β through the still operative c.e.a. feedback loop. The reduction in β, and hence current, in an operating region where the constant current controller is active calls for an increase in β. Thus an equilibrium is obtained between two antagonistic control loops, each with their contrary action upon β. $G_1(s)$ has been added to allow independent adjustment of gain and time constant of each system.

In the multiloop system, choosing two parameters becomes even more arbitrary: however, it was decided to leave the c.e.a. controller with a satisfactory setting and vary two parameters of $G_1(s)$. $G_2(s)$ was set to $\frac{30}{(1+0.5s)(1+0.1s)}$ and $G_1(s)$ was designated $\frac{K_1}{1+Ts}$. Again, instead of deriving expressions for $G_3(s)$ and $G_4(s)$ and reducing the block diagram to the overall transfer function, the relevant equations are written in matrix form. In this case the equations are those used for the c.e.a. case with the following modification to eqn (4.1):

$$\Delta V\varepsilon = -\ 9.6P_1\ \Delta\delta\ -\ 5P_3\ \cdot\ \frac{K_1}{1+Ts}\ \Delta I_d \tag{4.15}$$

For the same operating point the coefficient matrix becomes

$\Delta V\varepsilon$	$\Delta V\beta$	$\Delta\beta$	$\Delta\delta$	ΔI_d	ΔV_{di}
1+Ts			6.3(1+Ts)		K
30	$1+0.51s+0.05s^2$				
	0.214	1+0.008s			0.2+0.0016s
		0.252	0.165	1	
		-0.252	0.165		0.044
				1	0.205+0.06s

the determinant of which is

$$\begin{aligned} 0 = {} & 15.8 + 5.34K \\ & +(5.72 + 15.8T)s \\ & +(0.082 + 5.72T)s^2 \\ & +(0.0056 + 0.082T)s^3 \\ & +(0.00004 + 0.0056T)s^4 \\ & + 0.0004Ts^5 \end{aligned} \tag{4.16}$$

4.5 Transient c.e.a. Control

Due to the predictive nature of c.e.a. control, it is usual to compensate for a transient increase in current: when the current increases, the margin angle momentarily decreases, greatly increasing the risk of commutation failure. Hence a fast transient response is desirable and a non-optimal value of δ is tolerated for a short duration if overshoot occurs. However, a decrease in current and the momentary increase in margin requires a well-damped response of the controller to bring the margin angle back to the steady state value.

This asymmetrical control is produced by a current derivative signal which is active when the current increases and blocked when the current decreases. The circuit is shown in Fig. 4.14.

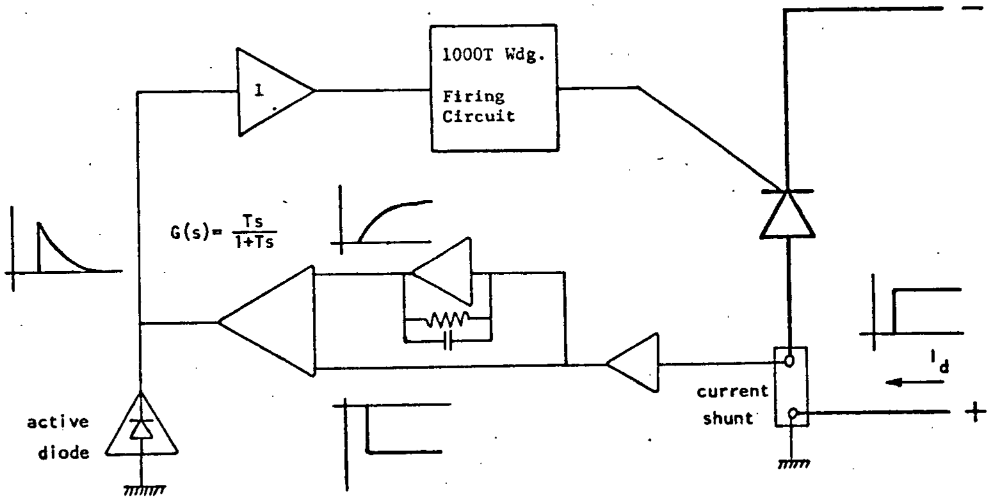

Fig 4.14. Transient c.e.a. Circuit

The output of Amplifier 1, zero at steady state, is connected to the 1000-turn winding of the firing circuit and summation with the c.e.a. control signal appears as the resultant m.m.f. in the saturable core. The effective time constant of this circuit should be significantly different than the effective time constant of the c.e.a. control loop.

In this chapter the inverter control implemenation was presented together with the mathematical description and derivation of the characteristic equation suitable for analysis using Siljak's method. The next chapter describes the application of this method to the controller in its two modes of control: constant extinction angle and constant current.

5. ANALYSIS AND EXPERIMENTAL RESULTS

This chapter describes the application of Siljak's method of parameter plane analysis to the comparison of the physical model in two ways:

1) by plotting the stability boundaries in the parameter plane and determining the experimental stability limit by adjusting the same two parameters in each case.

2) By photographing the response at different controller operating points and comparing the response to the damping factor according to the parameter plane plot.

The method may then be applied to determine the combination of parameters which produces best relative damping.

5.1 The Method of Siljak

The Siljak method of analysis [24,25,26] applies to the manipulation of the roots of the characteristic equation by two adjustable system parameters through the coefficients of the characteristic equation, written as

$$\sum_{k=0}^{n} a_k s^k = 0 \tag{5.1}$$

Where $s = \sigma + j\omega$ is the complex variable and a_k ($k = 0,1,2\text{--}n$), the real coefficients, are linear functions of two adjustable system parameters α and β:

$$a_k = \alpha b_k + \beta c_k + d_k \tag{5.2}$$

Following a small disturbance the system may execute oscillations of decreasing magnitude in returning to the equilibrium position. It is possible to define an undamped natural frequency ω_n and damping factor

ζ for these oscillations [21]

Substituting $\qquad s = -\omega_n\zeta + j\omega_n\sqrt{1-\zeta^2}$ $\qquad$ (5.3)

and applying the condition that the summation of real and imaginary parts must go to zero independently, (5.1) may be written

$$R = \mathcal{R}\,[\omega_n,\zeta,\alpha,\beta] = 0$$
$$I = \mathcal{I}\,[\omega_n,\zeta,\alpha,\beta] = 0 \qquad (5.4)$$

Equations (5.4) may be considered as two equations in two unknowns α and β which may be solved

$$\alpha = f(\omega_n,\zeta) \qquad \beta = g(\omega_n,\zeta) \qquad (5.5)$$

[provided that the Jacobian $J=J\,(R,I/\alpha,\beta)$ exists and is different from zero].

From these equations it is possible to map s-plane contours defined by ω_n,ζ into the parameter plane of α and β. For three cases, Fig. 5.1, the mapping functions may be derived analytically:

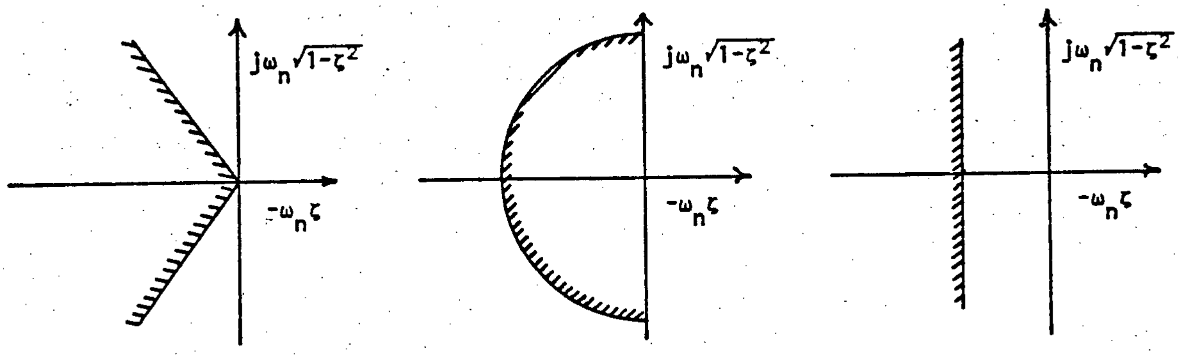

1. Constant Damping Factor ζ $\qquad$ 2. Constant Undamped Natural Frequency ω_n $\qquad$ 3. Constant Settling Time $\omega_n\zeta$

Fig 5.1 Contours which may be Mapped Into Parameter Plane

Numerical mapping of arbitrary s-plane contours is also possible using the method described in reference [27]. The result of mapping a number of s-plane contours into the parameter plane is a direct graphical technique of relating the root locations of the characteristic equation to two adjustable system parameters, such as gain, time constant etc...

The Siljak technique has the following characteristics:

(i) there is a definite advantage to the Mitrovic method in that the adjustable parameters may appear in any number of coefficients of the characteristic equation.

(ii) the relative stability, or other performance measure, may be directly related to a pair of system parameters.

(iii) two parameters may be simultaneously adjusted, providing a definite advantage over other algebraic domain methods where only one system parameter is adjustable.

(iv) the method has been extended by Siljak[26] so that parameters may appear non-linearly in the coefficients of the characteristic equation, and is useful where two adjustable parameters appear in different control loops of the system.

5.2 Application to Inverter System

The parameter plane mapping functions $\alpha = f(\omega_n,\zeta)$, $\beta = g(\omega_n,\zeta)$ for the characteristic equation (4.14) are derived analytically in Appendix B. From these functions it is possible to define areas of absolute stability by mapping the left half s-plane into the parameter plane, shown in Fig. 5.2.

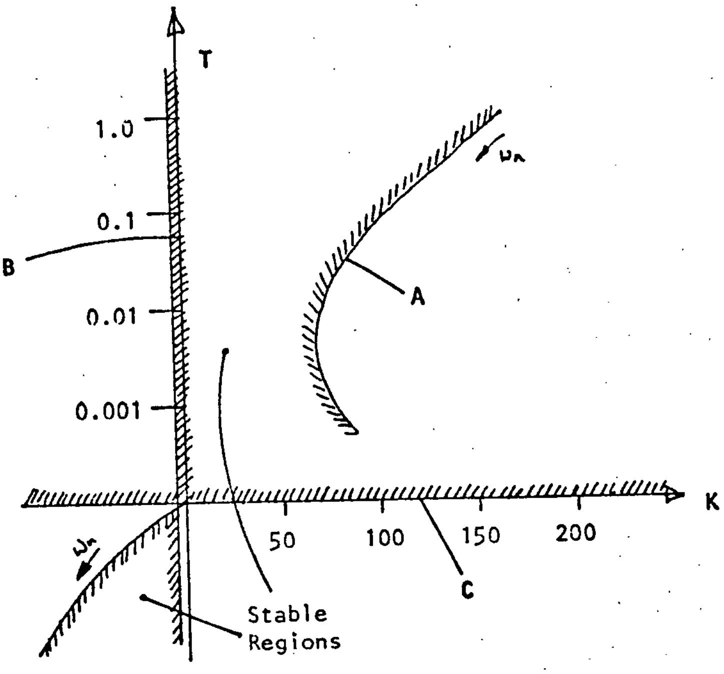

Fig 5.2 Regions of Absolute Stability

Segment 'A' corresponds to the imaginary axis or s=0 line and segments B and C respectively to the real root boundaries s=0 and s=∞. Shading of the curves emphasizes the regions of stability: in the direction of increasing ω_n shade on the left of the curve if $\Delta<0$ and on the right if $\Delta>0$ [see Appendix B]. That these areas correspond to four roots with negative real parts may be confirmed by applying the Routh-Hurwitz criterion: the characteristic equation at the point (50,0.1) becomes

$$3.5\times10^{-6}\ s^4 + 1\times10^{-4}\ s^3 + 8.3\times10^{-3}\ s^2 + 1.06s + 2.8 = 0 \tag{5.6}$$

The Routh-Hurwitz coefficient array is

2.8	8.4×10^{-3}	3.5×10^{-6}
1.06	5.1×10^{-4}	
7.47×10^{-3}	3.5×10^{-6}	
1.0×10^{-7}		
0		

There are no sign changes in the left hand column, indicating that all roots have negative real parts for values of K and T within the shaded boundaries of Fig. 5.2.

In the determination of the experimental stability limit the gain K was increased for a number of values of T until unstable oscillation occurred after a step input. At each point where instability occurred, the undamped frequency of oscillation was measured. By marking in values of ω_n on the theoretical curves and by plotting more constant-ζ curves a more complete picture of theoretical behaviour is obtained as in Fig. 5.3. The experimental stability limit is shown and may be compared to the ζ=o line. The parameter plane map shows that over a large range of gain K the system remains predominantly underdamped, a fact which corresponded with practical experience.

A further comparison may be made by photographing the oscillogram of the response at a number of operating points. Fig. 5.4 shows the photographed response at nine different operating points defined in Fig. 5.3.

A fairly close correspondence between theoretical and experimental behaviours is seen, and that the transient response follows a

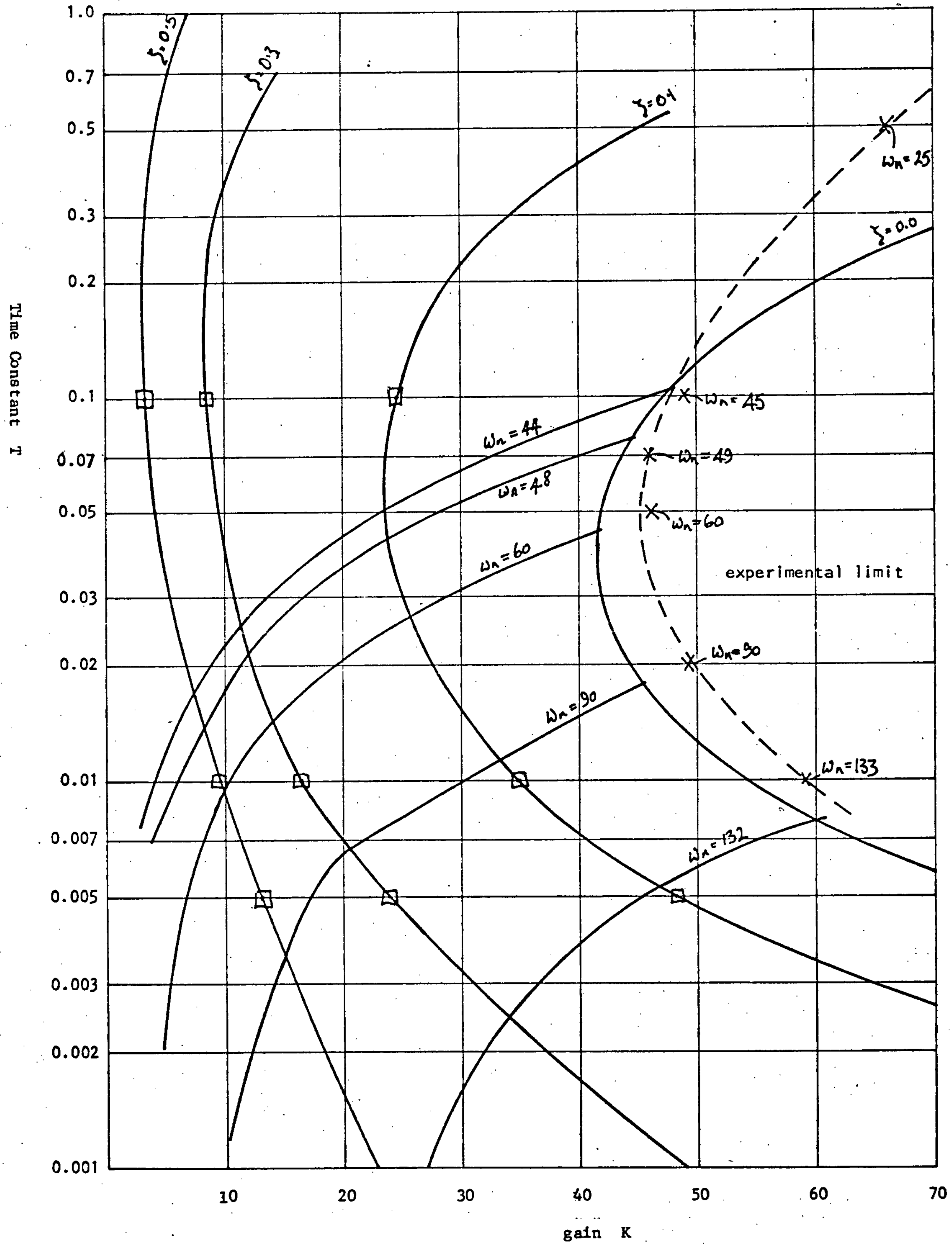

Fig 5.3 Constant ζ Curves for c.e.a. Controller

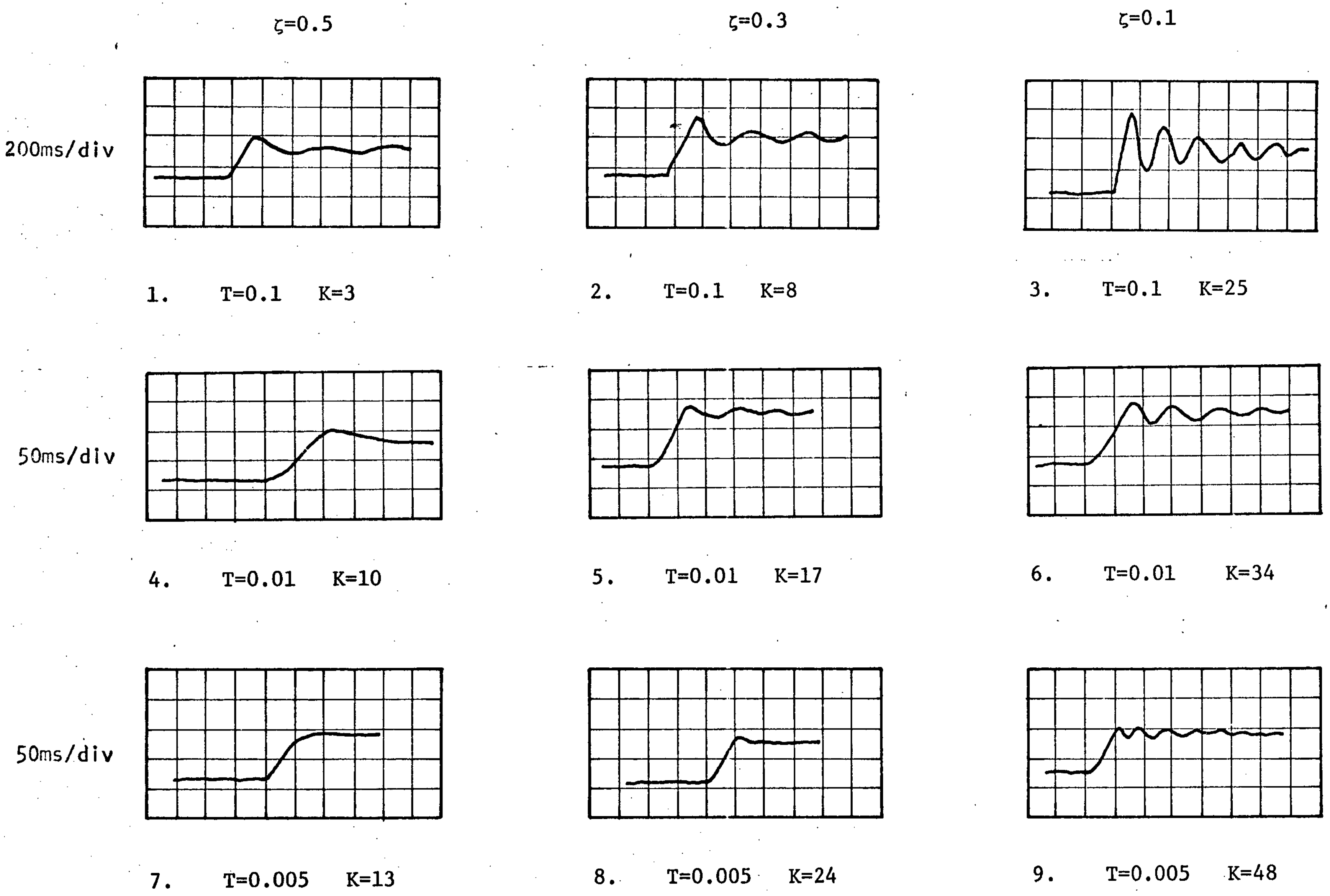

Fig 5.4 Photographed Responses at the Points Indicated in Fig 5.3

more predictable pattern as T increases, or ω_n decreases. More specifically the theoretical damping factors find closer agreement with the actual response as ω_n, or the system bandwidth, decreases. This would seem to suggest that the faster the response, i.e. the larger the bandwidth, the less valid linear continuous theory becomes, and hence the less reliable are predictions made by linear continuous techniques.

It should be emphasized that the error amplifier must provide enough filtering of the discontinuous δ feedback signal, since the time constants are effectively divided by the closed loop gain. Thus for small time constants and large values of gain the system does not exhibit less damping but imbalance of the firing pulses due to inadequate filtering.

An error amplifier with a single pole did not exhibit any correspondence to the linear model: oscillation only at large values of T and unbalanced firing at lower values of T.

Constant Current Control

In a similar manner the stability regions for the constant current controller may be derived for the characteristic equation (4.16), Fig. 5.5.

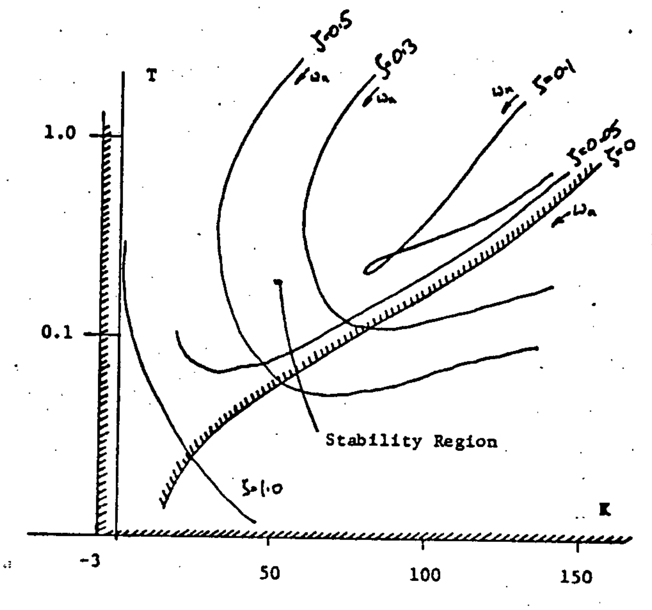

Fig 5.5
Stability Regions
For Constant
Current Control

The constant damping curves for the higher order system are found to be somewhat confusing due to the fold-over effect, indicating the existence of a number of complex roots. In selecting values of the variable parameters for best relative damping, the pair of roots with the lower damping factor is of primary interest: whatever the value of gain and time constant, the best that can be achieved is a largely underdamped control, a fact which corresponded very closely with the practical experience that control was extremely difficult to maintain at a stable operating point except at low values of gain and slow response time.

An alternative scheme for the analysis of constant current is shown in Fig. 5.6 where the two adjustable parameters are the values of gain in the feedback loops and the value of 30 is set for the gain of the error amplifier.

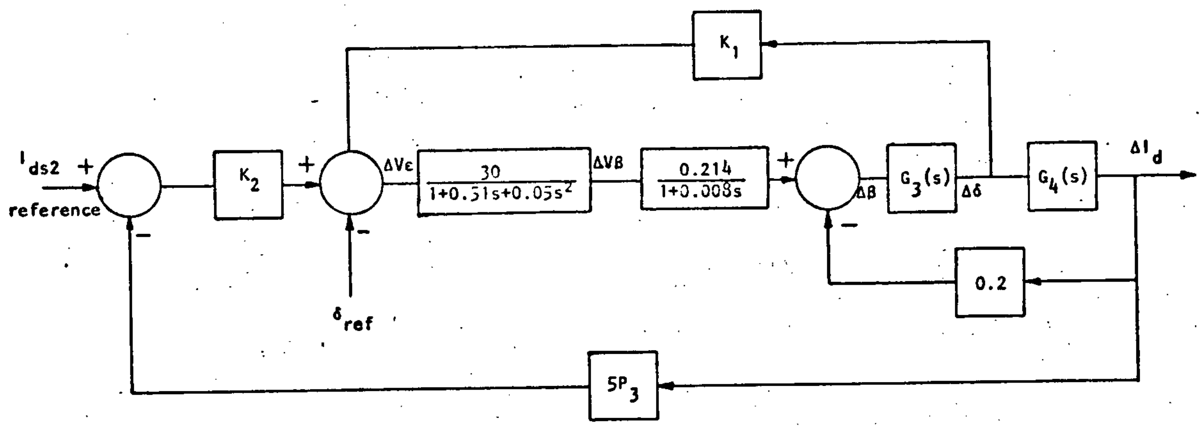

Fig 5.6 Alternate Scheme for Analysis

The characteristic equation in this case is

$$\begin{aligned} 0 = {} & 0.05 + 0.26K_1 + 0.53K_2 \\ & + (0.037 + 0.097K_1)s \\ & + (0.0074K_1)s^2 \end{aligned}$$

$$+ 0.0005\ s^3$$
$$+ 3.6\text{x}10^{-4}\ s^4 \qquad (5.6)$$

The parameter plane curves are shown in Fig. 5.7.

Setting $K_2 = 0$ and $K_1 = 6.3$ the point A in Fig. 5.7 corresponds to the point K=30, T=0.1 in Fig. 5.3, with a damping factor between 0 and 0.1. The introduction of the additional feedback signal again produces an underdamped system until the values of gain are reduced. Any change in K_1 must be cross-checked with Fig. 5.3.

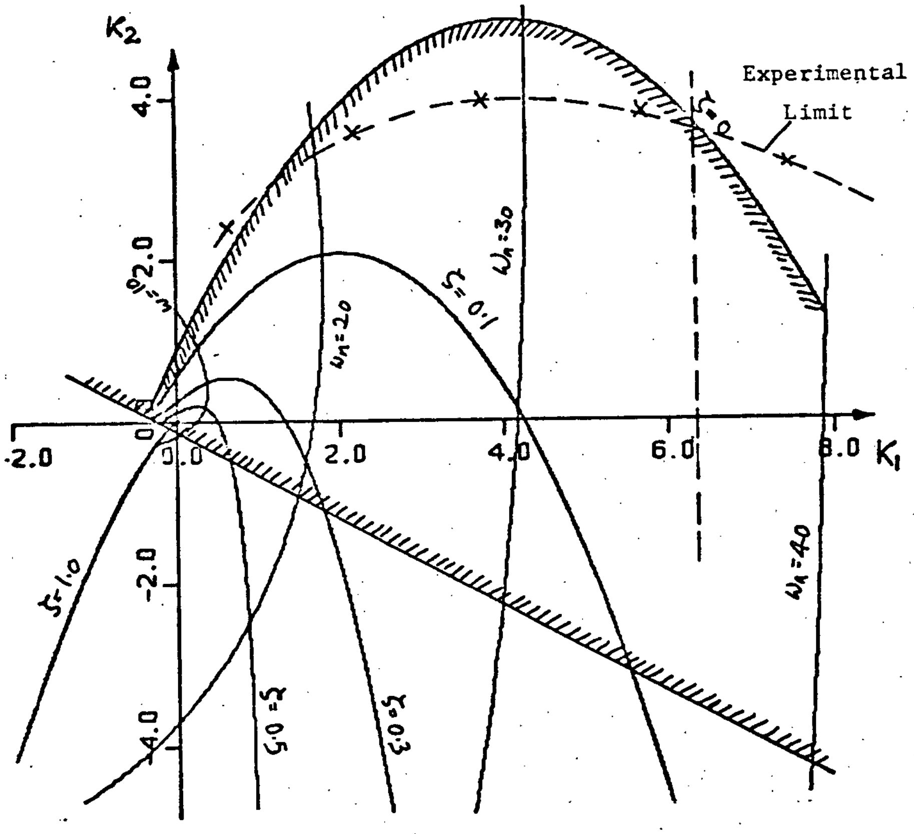

Fig 5.7 Characteristic Curves For Eqn (5.6)

6. RECTIFIER CONTROL

Under normal conditions, the rectifier operates on either constant current control or constant power control: overall control of the rectifier operation is maintained by fast electronic control of firing angle α, responding to spontaneous fluctuations within the system, and the slower electromechanical on-load tap changer, which serves to maintain the firing angle within prescribed operating limits[14,47]. The upper limit is imposed to minimize reactive power consumption at the rectifier and the lower limit of α provides a margin for a rapid increase in power demand by α control only. This lower limit is usually larger than another (lowest possible) limit ($\alpha > o$) which ensures the simultaneous firing and equal load sharing of a number of anodes in parallel. If, due to fluctuations of voltage at the sending end a.c. system, the firing angle is brought to a limiting value, then normal control action is to bring the tap changer into operation, after an appropriate delay to accommodate transients. For example, if the a.c. voltage fell to a new low value, then α is taken past its lower limit in order to maintain constant current or constant power. Tap changer action to increase the secondary/primary turns ratio allows the electronic control to bring α back to its normal operating range.

In the model, however, the tap changer was found to be unnecessary and unusable at this stage of development, and the turns ratio adjustment was accomplished manually using a three phase power variac at each converter station. The remainder of this chapter presents the implementation of two rectifier controls: constant - α and constant current. The last section describes other forms of rectifier control and suggests how they might be implemented.

Again the DONNER Analog Computer was used for the controller.

6.1 Constant α control

Advantageous use may be made here of the extinction angle detector circuit described in section 4.2. This same circuit may be used to detect the firing angle α and derive a feedback signal for the constant-α control shown in Fig. 6.1.

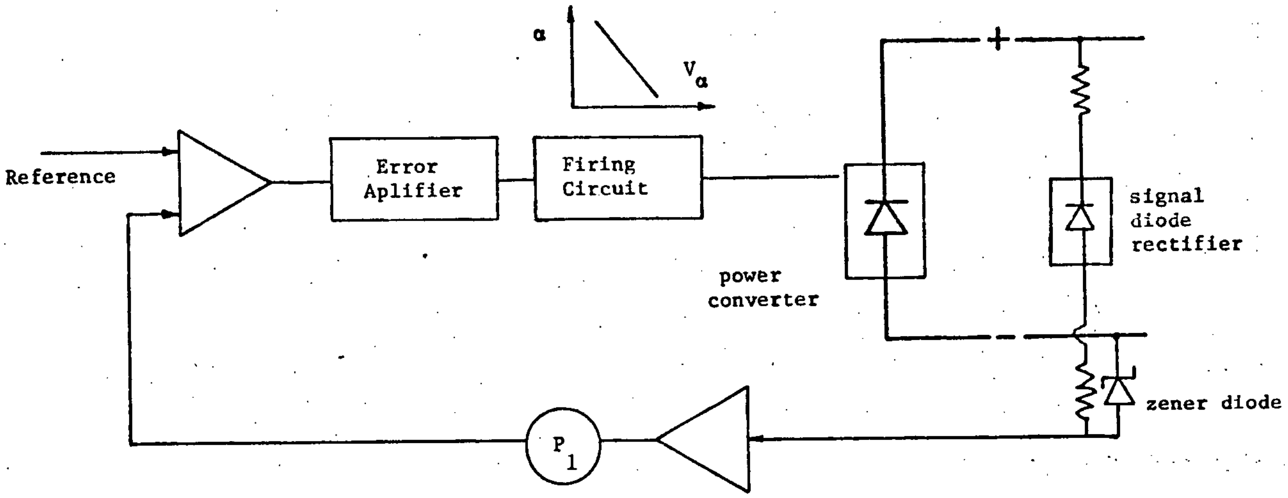

Fig 6.1 Rectifier Constant-α Control

The constant-α controller shown above differs from the constant extinction angle controller shown in Fig. 4.10 only in the sense of the signal diode bridge rectifier with respect to the converter terminals. The equations are slightly different since the angle detected is the firing angle itself and not some angle related to it through the power circuit. From the block diagram in Fig. 6.2 five equations may be written:

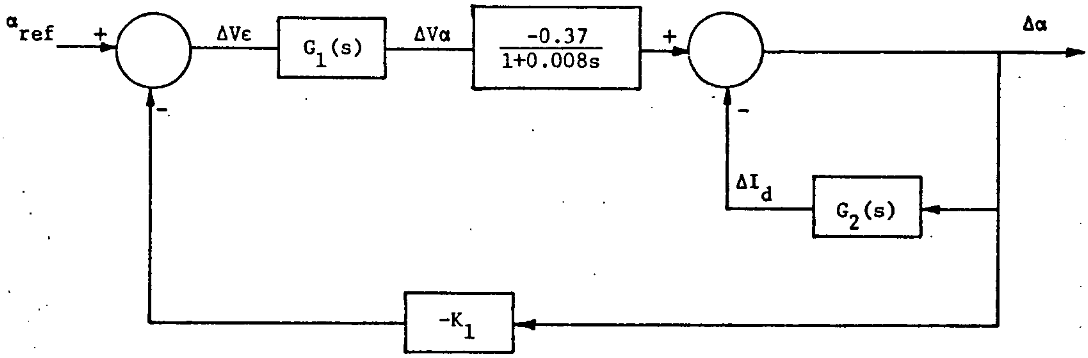

Fig 6.2 Constant-α Block Diagram

Three control equations:

$$\Delta V\varepsilon = K_1\Delta\alpha \tag{6.1}$$

$$\Delta V\alpha = G_1(s)\ \Delta V\varepsilon \tag{6.2}$$

$$\Delta\alpha = \frac{-.37}{1+0.008s}\ \Delta V\alpha - G_2(s)\Delta I_d \tag{6.3}$$

Two power equations

$$V_{dr} = V_{dor}\ \cos\alpha - \frac{3}{\pi}X_c I_d \tag{6.4}$$

$$I_d(R_{dc} + sL_{sm}) = V_{dv} - V_{di} \tag{6.5}$$

from which $$\Delta V_{dr} = -V_{dor}\ \sin\alpha\ \Delta\alpha - \frac{3}{\pi}X_c\Delta I_d \tag{6.6}$$

assuming V_{dor} remains constant, and

$$\Delta I_d(R_{dc} + sL_{sm}) = \Delta V_{dr} - \Delta V_{di} \tag{6.7}$$

Unfortunately V_{di} does not remain constant, and since the rectifier cannot be operated in 'hvdc mode' without a regulated inverter, these equations should be used in conjunction with those describing the appropriate behaviour of the inverter. In this case, constant-α control at the rectifier implies constant current mode at the inverter.

6.2 Constant Current Control

The constant current loop is the primary regulator for the rectifier. It is added to the constant-α controller with a clamp to limit the feedback signal when the current falls below the setting I_{ds1}. The circuit, shown in Fig. 6.3, allows independent adjustment of α_{min} and I_{ds1}. It should be noted that α is limited at its lowest permissible value and not at the two operating limits at which the tap changer would operate. The block diagram is shown in Fig 6.4.

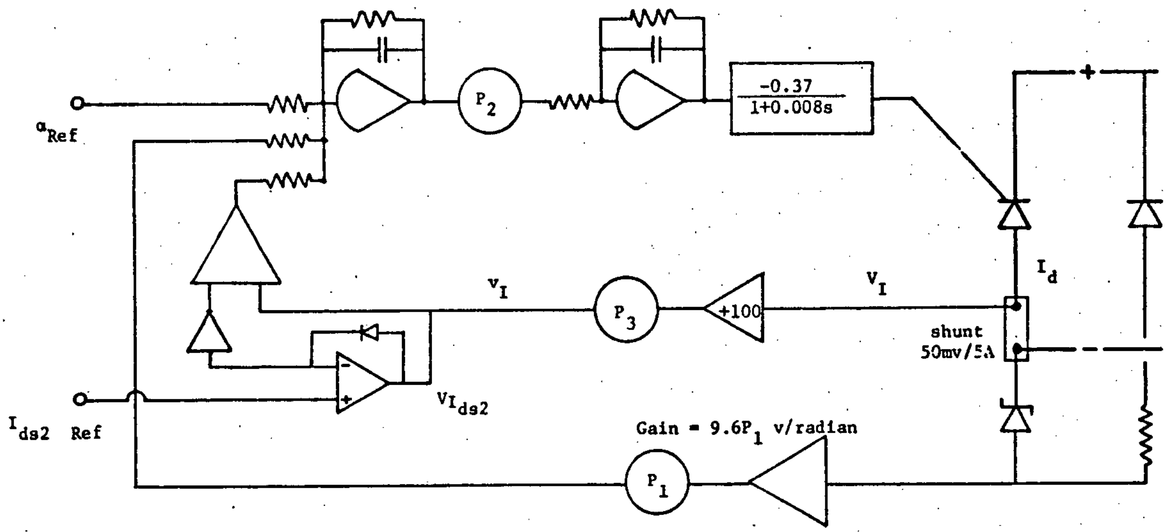

Fig 6.3 Circuit for Rectifier Constant Current and Constant-α Controllers

Equation (6.1) becomes

$$\Delta V\varepsilon = K_1\Delta\alpha - K_2\Delta I_d \tag{6.8}$$

6.3 Operation of the d.c. link

Operation of the d.c. link in two modes is now possible:

(1) Rectifier in c.c. mode, inverter in c.e.a. mode.

(2) Rectifier in constant-α mode, inverter in c.c. mode.

The operating procedure is to start up the link without regulation to a low current operating point, then the controllers are applied and the link brought up to the required operating point.

The operation of the link with the controllers described in this text was found to be stable but underdamped, thus requiring compensation. By using single pole error amplifiers the link acquires considerable stability, but linear continuous models do not apply.

6.4 Other Forms of Converter Control

Constant power control was easily implemented using the multiplier available with the DONNER analog computer. In application to the model it should be used in conjunction with a constant current override for overcurrent protection.

Another type of control, suggested by Machida and Yoshida [48] is to control the frequency of a weak a.c. system by fast control of power in a d.c. link of comparable size.

Where reactive power compensation is accomplished by switching capacitors, constant reactive power control has been suggested by Kanngeisser[51], again for use with weak a.c. systems.

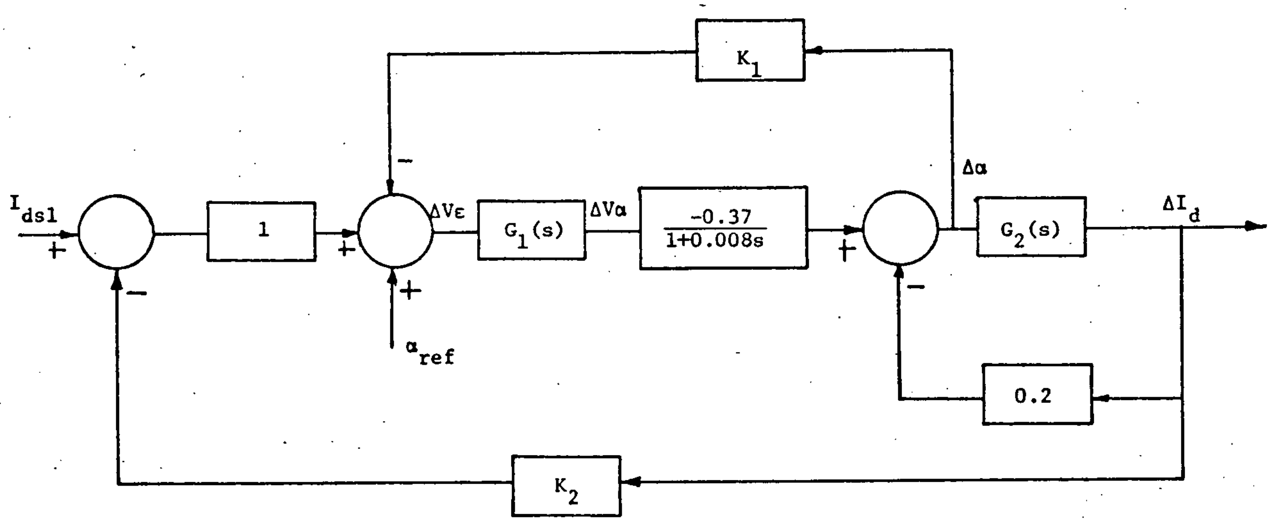

Fig 6.4 Constant Current Controller Block Diagram

7. DISCUSSION AND CONCLUSION

This concludes the study. The physical model has been shown to simulate the steady-state operation of a d.c. link when connected between two points in a strong a.c. system. The control systems have been built using the differential amplifiers of an analog computer. Hence they can easily be changed to the mode of control required by the experimenter. Whatever the mode of control for the inverter, it must always be provided with a constant/minimum extinction angle override for protection against commutation failure. The novel extinction angle detector, designed by the author, is ideally suited to the model, and may, without too much difficulty be applied to a full-sized converter. The only change from c.e.a. control for inversion to constant α for rectification is the change in sense of the signal diode three-phase rectifier connected across the terminals of the power converter.

Further application of the model to the study of generator - d.c. link - infinite bus, or parallel a.c. - d.c. transmission would require the addition of a.c. harmonic filters. The per-unit reactive power provided may then be varied by changing either the components of the filter or the rating of the link.

With respect to the mathematical description and its correspondence with the physical model, the assumption that the converter system is linear and continuous is valid only for small perturbations and small system bandwidth. When both conditions were fulfilled, then the analysis using Siljak's method was found to be quite accurate. However in the analysis of fault response and transient response, both assumptions must be discarded, as perturbations are far from small and effective control response must occur within the period of a few successive firings[38]. Also, the contemporary trend is to apply d.c. links in situations where their high bandwidth capabilities are fully realized, eg. parallel a.c. - d.c. transmission, weak a.c. systems. The analysis has shown that the linear continuous assumption is unsuitable for such applications. Figs. 5.3 and 5.4 indicate that the damping curves reflect the system behaviour at slow frequency of response, becoming more inaccurate as the frequency increases.

In the actual practice of application, the Siljak method of stability analysis appears as restricted as one-parameter methods for the relative stability optimization of a number of parameters in a control system. Since all parameters must be simultaneously adjusted, the two dimensional graphical technique becomes laborious when three or more parameters are required to be adjusted.

With respect to the further development of the model, the physical limitation to the achievement of a fast stable response is the firing circuit, which, in order to maintain balanced firing pulses, requires the feedback signal to be low-pass filtered, inevitably slowing response time.

This 'equal-angle' firing circuit is also unbalanced by asymmetrical phase conditions, affected by commutation distortion of phase voltages and sensitive to changes in supply voltage. Under single-phase a.c. fault conditions, control is sometimes maintained by asymmetrical firing of the valves, not possible with the present firing circuits. Also the rapid reversal of power flow is not possible due to the restricted range of firing pulse variation. Since the flexibility of the d.c. link is the flexibility of its electronic control system, the firing circuit, as an essential part of the control system, is seen as a major limitation of the physical model.

REFERENCES

1. E.S. Groiss, A. V. Posse, V.E. Touretski, "800kV D.C. Transmission System Stalingrad-Donbass", CIGRE Paper 414, 1960.

2. G.D. Brewer, E.M. Hunter, P.G. Engstrom, R.F. Stevens, "Celilo Converter Station of the Pacific h.v.d.c. Intertie", IEEE Transactions on Power Apparatus and Systems, Vol PAS-85, No 11, Nov 1966, pp 1116-1128.

3. K.L. Hurdle, C. MacGregor, T.E. Storey, "The Selection of $\pm$450kV d.c. for the Transmission of Power from the Nelson River", Engineering Journal Vol 50, No 10, Oct 1967, pp 17-20.

4. T.E. Calverley, "Development in D.C. Transmission", Transactions of the Sourth African Institute of Electrical Engineers, Vol 59, Part 7, July 1967, pp 133-163.

5. P.J. Croft, H.M. Ellis, "D.C. Transmission to Boost Vancouver Island Supply", Electrical World, May 31, 1965, pp 44-47.

6. B.J. Cory, "High Voltage Direct Current Converters and Systems", MacDonald 1965, Chap. 8, pp 175-218.

7. Ibid, Chap 5, p 91.

8. Ibid, Chap 7, p 145.

9. Ibid, Chap 8, pp 165-173.

10. Ibid, Chap 4, pp 44-72.

11. Ibid, Chap 9, p 236.

12. S. Fukunda, I. Takei, "The Sukuma D.C. Frequency Converter Project", Direct Current, Vol 7, 1964.

13. J.D. Ainsworth, "The Phase-locked Oscillator - A New Control for Controlled Static Converters", IEEE Transactions on Power Apparatus and Systems, Vol PAS-87, No 3, March 1968, pp 859-865.

14. A. Ekstrom, G. Liss, "A Refined HVDC Control System", IEEE Trans. on Power Apparatus and Systems, Vol PAS-89, May 1970, pp 723-732.

15. E. Uhlmann, "Stabilisation of an AC Link by a Parallel DC Link", Direct Current, Aug 1964, pp 89-94.

16. J.J. Dougherty, "Operating Characteristics of a Three-Terminal DC Transmission Line", IEEE Summer Power Meeting, Dallas, Texas, June 22-27, 1969.

17. J.P. Bowles, B.J. Cory, "The Model hvdc Transmission System at Imperial College, London", Direct Current, Sept 1963, pp 236-240.

18. J.D. Ainsworth, J.P. Bowles, "An HVDC Simulator Suitable for both Steady-State and Transient Studies", IEE Proc. Conference No 22 on HVDC Transmission, 1966, Paper 25.

19. J.J. Dougherty, V. Caleca, "The EEI AC/DC Transmission Model", IEEE Trans. on Power Apparatus and Systems, Vol PAS-87, No 2, Feb 1968, pp 504-512.

20. G. Gordon, "System Simulation", Prentice Hall, 1969.

21. G.J. Thaler, R.G. Brown, "Analysis and Design of Feedback Control Systems", McGraw-Hill 1960, Chap 4, p 105.

22. K. Eriksson, G. Liss, "Stability Analysis of the HVDC Transmission Control System Using Theoretically Calculated Nyquist Diagrams", IEEE Trans. on Power Apparatus and Systems, Vol PAS-89, No 5, May/June 1970, pp 733-739.

23. J. Clade, A. Lacoste, "Simplified Study of The Stability of Regulation of a D.C. Link", Direct Current, Feb 1967, p 9-22.

24. D.D. Siljak, "Analysis and Synthesis of Feedback Control Systems in the Parameter Plane, 1 - Linear Continuous Systems", IEEE Trans. (Applications and Industry), Vol 83, Nov 1964, p 449-458.

25. D.D. Siljak, "Generalisation of the Parameter Plane Method", IEEE Trans. on Automatic Control, Vol AC-11, No 1, Jan 1966, pp 63-70.

26. D.D. Siljak, "Non-Linear Systems", John Wiley & Sons, 1969.

27. Ibid Appendix B, pp 411-2.

28. N.N. Hancock, "Electric Power Utilisaion", Pitman 1967, pp 320-339.

29. J. Schaeffer, "Rectifier Circuits, John Wiley & Sons, 1968.

30. A.J. Wood, S.B. Gray, C. Concordia, "An Economic Study of D.C. versus A.C. Overhead Transmission", AIEE Trans. on Power, Vol 78, No 6, June 1959, pp 338-349.

31. L.R. Neiman and Others(Editors), "D-C Transmission in Power Systems", Israel Program for Scientific Translations, 1967, p 59.

32. C. Adamson, N.G. Hingorani, "High Voltage Direct Current Power Transmission", Garraway, 1960, pp 159-166.

33. Ibid, Chap 10, p 143.

34. J.D. Ainsworth, "Harmonic Instability Between Controlled Static Converters and A.C. Networks", Proc IEE, Vol 114, No 7, July 1967, pp 949-957.

35. J.C. Read, "The Calculation of Rectifier and Inverter Performance Characteristics", Proc IEE, Vol 92-11, pp 495-509.

36. D.E. Fletcher, C.D. Clarke, "A.C. Filters for the Nelson River Project", Manitoba Power Conference on EHV-DC, June 1971, Winnipeg, Manitoba.

37. J.P. Bowles, "Control Systems for High Voltage Direct Current Transmission", Spring Meeting, CEA, Vancouver 1971.

38. G.L. Brewer, C.D. Clarke, A. Gavrilovic, "Design Considerations for A.C. Filters", IEE Proc. on HVDC Transmission, 1966, Paper 56.

39. E. Friedlander, "Features of Static Reactive Power Supply for Polyphase Converters", Proc. IEE Conference on HVDC Transmission, 1966, Paper 54.

40. H.A. Calderbank, J.S. Colls, "Compensation for D.C. Transmission with Particular Reference to Synchronous Converters", Proc. IEE Conference on HVDC Transmission, 1966, Paper 53.

41. F. Ileceto, "D.C. link and A.C. Network Combined Power Requirements", Direct Current, May 1964, pp 147-155.

42. C. Adamson, N.G. Hingorani, "Control of h.v.d.c. Converters", Direct Current, June 1962, pp 147-155.

43. General Electric Company SCR Manual, 1967 Edition.

44. Ibid, p 304.

45. Firing Circuits Inc., "SCR Controls", Bulletin 5001, Nov 1967.

46. Three-Phase Full Wave SCR Firing Circuit Application Drawing 1241-3003C, Firing Circuits Inc., Connecticut.

47. N.G. Hingorani, P. Chadwick, "A New Constant Extinction Angle Control for Static AC/DC/AC Converters", IEEE Trans. on Power Apparatus And Systems, Vol PAS-87, No 3, March 1968, pp 866-872.

48. T. Machida, Y. Yoshida, "A Method to Detect The De-ionisation Margin Angle and to Prevent the Commutation Failure of an Inverter for D.C. Transmission", IEEE Trans. on Power Apparatus and Systems, Vol PAS-86, No 3, March 1967, pp 259-262.

49. J. Arrillaga, G. Galanos, E.T. Powner, "Direct Digital Control of HVDC Converters", IEEE Trans. on Power Apparatus and Systems, Vol PAS-89, No 8, Nov/Dec 1970, pp 2056-2065.

50. L.A. Bateman, R.W. Haywood, R.F. Brooks, "Nelson River D.C. Transmission Project", IEEE-EHV Transmission Conference Proceedings, 1968, Paper 18.

51. K.W. Kanngi-sser, H.D. Lips, "Control Methods to Improve the Reactive Power Characteristics of HVDC Links", IEEE Transactions on Power Apparatus and Systems, Vol PAS-89, No 6, July 1970, pp 1120-5

52. B.J. Kabriel, personal conversations

APPENDIX A

(a) Computation of Characteristic Equation

While the algebraic description of the method is lengthy and cumbersome, its simplicity in principle is best illustrated by example: consider the following 3x3 matrix

$$M = \begin{bmatrix} s^2 + K_1 s + 3 & s + 2 & 0 \\ 0 & s + K_2 & s + K_1 \\ s + 1 & 0 & s + 4 \end{bmatrix}$$

where K_1 and K_2 are algebraic variables. Expanding along the third row

$$\begin{aligned} \Delta &= (s+1)(s+2)(s+K_1) + (s+4)(s+K_3)(s^3+K_1 s+3) \\ &= s^4 + (5+K_1+K_2)s^3 + (6+5K1+4K_2+K_1K_2)s^2 + (14+3K_1+3K_2+4K_1K_2)s \\ &\quad + 2K_1 + 12K_2 \end{aligned} \tag{4.1}$$

The first step in the computer program is to compute the determinant of numerical terms only i.e. determinant of M above with coefficients of the algebraic variables omitted

$$A = \begin{vmatrix} s^2 + 3 & s + 2 & 0 \\ 0 & s & s \\ s + 1 & 0 & s + 4 \end{vmatrix}$$

$$= s(s+1)(s+2) + s(s^2+3)(s+4)$$

$$= s^4 + 5s^3 + 6s^2 + 14s$$

It is noted that two algebraic variables occur in three positions $K_1(1,1)$, $K_1(2,3)$, $K_2(2,2)$. For each variable position in turn eliminate all terms in that row and column except the variable and its coefficient. For K_1 in position (1,1) the modified determinant becomes

$$B_{K_1} = \begin{vmatrix} K_1S & 0 & 0 \\ 0 & s & s \\ 0 & 0 & s+4 \end{vmatrix} = K_1(s^3 + 4s^2)$$

For K_1 in position (2,3)

$$C_{K_1} = \begin{vmatrix} s^2+3 & s+2 & 0 \\ 0 & 0 & K_1 \\ s+1 & 0 & 0 \end{vmatrix} = K_1(s^2 + 3s + 2)$$

For K_2 in position (2,2)

$$D_{K_2} = \begin{vmatrix} s^2+3 & 0 & 0 \\ 0 & K_2 & 0 \\ s+1 & 0 & s+4 \end{vmatrix} = K_2(s^3 + 4s^2 + 3s + 12)$$

Next where 2 algebraic variables occur in 2 positions, each with a different row and column, the same rule applies for each position:

For K_1 in M(1,1) and K_2 in M(2,2)

$$E_{K_1K_2} = \begin{vmatrix} K_1S & 0 & 0 \\ 0 & K_2 & 0 \\ 0 & 0 & s+4 \end{vmatrix} = K_1K_2(s^2+4s)$$

For K_1 in M(1,1) and K_1 in M(2,3)

$$F_{K_1{}^2} = \begin{vmatrix} K_1s & 0 & 0 \\ 0 & 0 & K_1 \\ 0 & 0 & 0 \end{vmatrix} = 0$$

The possibilities having been exhausted the determinant of the matrix M is

$$\begin{aligned}\Delta &= A + B_{K_1} + C_{K_1} + D_{K_2} + E_{K_1K_2} + F_{K_1}{}^{2}\\ &= s^4 + 5s^3 + 6s^2 + 14s\\ &\quad + K_1s^3 + 5K_1s^2 + 3K_1s + 2K_1\\ &\quad + K_2s^3 + 4K_2s^2 + 3K_2s + 12K_2\\ &\qquad + K_1K_2s^2 + 4K_1K_2s\end{aligned}$$

$$\begin{aligned}&= s^4 + s^3(5 + K_1 + K_2) + s^2(6 + 5K_1 + 4K_2 + K_1K_2)\\ &\quad + s(14 + 3K_1 + 3K_2 + 4K_1K_2) + 2K_1 + 12K_2\end{aligned}$$

which is equal to equation (4.1). This principle may be applied to matrices with more than two algebraic variables and may be extended to the computation of completely algebraic determinants.

(b) Determinant program

The program written in FORTRAN H resides in the file UEFG: CHAREQN and is invoked with the following command:

$RUN UEFG:CHAREQNH 5=file 1 6=file 2 7=file 3

where

file 1 is the input file containing data in the format (G20.7, 4I5) one data card or line is required for each term in each matrix element: eg. the term $s^2 + 3K_1s + 2$ in position (1,1) would require 3 cards:

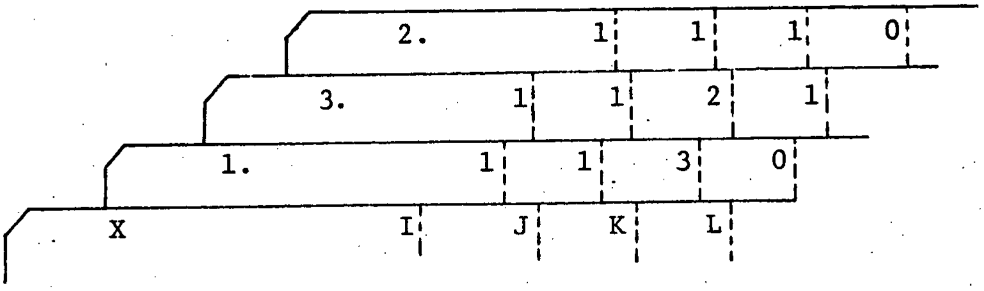

where X is the coefficient

(I,J) are the row and column of the term

K is the index which represents the power of s of which X is the coefficient

$s^0 \equiv 1$ $s^1 \equiv 2$ $s^2 \equiv 3$ etc.

L is the number of the algebraic variable all of which are denoted K_L.

File 2 is the file or device for the point out of the solution, the input data is echo printed on unit 6.

File 3 is the file into which data is written for reading by the program which computes the Siljak curves.

For the example given in part A, the input data appears as

1	1.	1	1	2	1
2	3.	1	1	1	
3	1.	1	1	3	
4	2.	1	2	1	
5	1.	1	2	2	
6	1.	2	2	2	
7	1.	2	2	1	2
8	1.	2	3	2	
9	1.	2	3	1	1
10	1.	3	1	1	
11	1.	3	1	2	
12	1.	3	3	2	
13	4.	3	3	1	

And the output, equal to (A.1) and (A.2).

```
CONSTANT TERM(S)
                                   K1:        2.000000000
                                   K2:        12.00000000

                     1
COEFFICIENTS OF S                              14.00000000

                                   K1:        3.000000000
                                   K2:        3.000000000
                                K1*K2:        4.000000000
```

COEFFICIENTS OF S^2		6.000000000
	K1:	5.000000000
	K2:	4.000000000
	K1*K2:	1.000000000
COEFFICIENTS OF S^3		5.000000000
	K1:	1.000000000
	K2:	1.000000000
COEFFICIENTS OF S^4		1.000000000

APPENDIX B: COMPUTATION OF SILJAK CURVES

Consider the characteristic equation

$$f(s) = \sum_{k=o}^{m} a_k s^k = o \tag{B.1}$$

using the usual notation; if s is expressed as

$$s = -\omega_n \zeta + j\omega_n \sqrt{1 - \zeta^2} \tag{B.2}$$

where ω_n is the undamped natural frequency, then it has been shown that powers of s may be expressed concisely as

$$s^k = \omega_n{}^k\{(-1)^k T_k(\zeta) + j\sqrt{1 - \zeta^2}(-1)^{k+1}\, U_k(\zeta)\} \tag{B.3}$$

where $T_k(\zeta)$ and $U_k(\zeta)$ may be obtained by the recurrence formulae

$$\begin{aligned} T_{k+1}(\zeta) - 2\zeta T_k(\zeta) + T_{k-1}(\zeta) &= 0 \\ U_{k+1}(\zeta) - 2\zeta U_k(\zeta) + U_{k-1}(\zeta) &= 0 \end{aligned} \tag{B.4}$$

with $T_o(\zeta) = 1$, $T_1(\zeta) = \zeta$, $U_o(\zeta) = 0$ and $U_1(\zeta) = 1$

Substitution of equation (B.3) into (B.1) and separation of real and imaginaries which must both independently go to zero enables equation (B.1) to be rewritten:

$$\begin{aligned} &\sum_{k=o}^{n} (-1)^k\, a_k \omega_n{}^k T_k(\zeta) = 0 \\ &\sum_{k=1}^{n} (-1)^{k+1}\, a_k \omega_n{}^k\, U_k(\zeta)\sqrt{1 - \zeta^2} = 0 \end{aligned} \tag{B.5}$$

Now, the coefficients a_k of the characteristic equation 1 appear as linear functions of variable system parameters α and β.

$$a_k = b_k\alpha + c_k\beta + d_k \tag{B.6}$$

equations D.5 are then able to be rewritten

$$\alpha B_1(\omega_n,\zeta) + \beta C_1(\omega_n,\zeta) + D_1(\omega_n,\zeta) = 0$$
$$\alpha B_2(\omega_n,\zeta) + \beta C_2(\omega_n,\zeta) + D_2(\omega_n,\zeta) = 0 \qquad (B.7)$$

where

$$B_1 = \sum_{k=o}^{n} (-1)^k\ b_k\omega_n{}^kT_k(\zeta) \qquad B_2 = \sum_{k=o}^{n} (-1)^{k+1}\ b_k\omega_n{}^k\sqrt{1-\zeta^2}\ U_k(\zeta)$$

$$C_1 = \sum_{k=o}^{n} (-1)^k\ c_k\omega_n{}^kT_k(\zeta) \qquad C_2 = \sum_{k=o}^{n} (-1)^{k+1}\ c_k\omega_n{}^k\sqrt{1-\zeta^2}\ U_k(\zeta)$$

$$D_1 = \sum_{k=o}^{n} (-1)^k\ d_k\ n^kT_k(\zeta) \qquad D_2 = \Sigma(-1)^{k+1}\ d_k\omega_n{}^k\sqrt{1-\zeta^2}\ U_k(\zeta)$$

$$(B.8)$$

Equations B.6 may be solved for unknowns α and β.

$$\alpha = \frac{1}{\Delta}[C_1D_2 - C_2D_1]$$
$$\beta = \frac{1}{\Delta}[B_2D_1 - B_1D_2] \qquad (B.9)$$

where $\Delta = B_1C_2 - B_2C_1$

For the characteristic equation 4.13, the mapping functions $\alpha = \alpha(\omega_n\zeta)$, $\beta = \beta(\omega_n\zeta)$ are derived analytically

$$B_1 = 0.547\ T_o(\zeta) - 0.203\ \omega_nT_1(\zeta)$$

$$B_2 = -0.547\ U_1(\zeta) + 0.203\ \omega_nU_1(\zeta)$$

$$C_1 = -0.577\ \omega_nT_1(\zeta) + 0.363\ \omega_n{}^2T_2(\zeta) - 0.047\ \omega_n{}^3T_3(\zeta) + 0.00036\omega_n{}^4T_4(\zeta)$$

$$C_2 = 0.577\ \omega_nU_1(\zeta) - 0.363\ \omega_n{}^2U_2(\zeta) + 0.047\ \omega_n{}^3U_3(\zeta) - 0.00036\omega_n{}^4U_4(\zeta)$$

$$D_1 = 0.577\ \omega_nT_o(\zeta) - 0.363\ \omega_nT_1(\zeta) + 0.047\ \omega_n{}^2T_2(\zeta) - 0.00036\omega_n{}^3T_3(\zeta)$$

$$D_2 = 0.577\ \omega_nU_o(\zeta) + 0.363\ \omega_nU_1(\zeta) - 0.047\ \omega_n{}^2U_2(\zeta) + 0.00036\omega_n{}^3U_3(\zeta)$$